INVESTIGATING NON-LINEAR FLUID STRUCTURE INTERACTION DYNAMICS USING INVISCID FLOW SOLVERS

PROJECT REPORT SUBMITTED BY

ARKA MAITY

RAJANYA CHATTERJEE

RITO BRATA NATH

RUPSAGAR CHATTERJEE

SNEHAL PATEL

UNDER THE GUIDANCE OF

Dr. SAYAN GUPTA

DEPARTMENT OF APPLIED MECHANICS, IIT MADRAS

&

Dr. SUNETRA SARKAR

DEPARTMENT OF AEROSPACE ENGINEERING, IIT MADRAS

ACKNOWLEDGEMENT

We are very grateful to Professor Sayan Gupta and Professor Sunetra Sarkar for providing us the opportunity to work as summer interns under their guidance. It is their continuous support, encouragement and constant zeal for excellence that has motivated us to go deeper in search for solution of the different arduous challenges and problems posed by the project.

We are greatly thankful to Chandan Bose of 'The Uncertainty Lab', IIT Madras, for his invaluable advices and insights throughout the project work and for his out-of-the-box thoughts and wits which were, indeed, a constant source of motivation all along.

We are also thankful to all the research fellows of 'The Uncertainty Lab', IIT Madras, for providing us a wonderful time and a very educative environment of work. Without their friendly co-operation, this project would have never been such an interesting undertaking.

ABSTRACT

The interaction between fluid flow past a structure and the associated dynamics have widespread significance and applications. Many of the today's daily life modern world utilities are based on the scientific knowledge derived from the study of fluid structure interaction. Some such noteworthy practical applications are design of aircraft wings, design of high speed cars, blood flow through arteries, design of MAVs and occurrence of aero-elastic fluttering.

A considerable number of physical phenomena in nature exhibit non-linear dynamics. And as such, a number of non-linear structural models (like Brennan's insect flight model, dipteran flight model with irrational non-linearity and, non-linear aero-elastic model having pitch and plunge degrees of freedom) have been adopted in the present study to model elements from the physical world. Panel methods (namely, Lumped Vortex Method and Unsteady Vortex Lattice Method) have been taken up for the evaluation of the flow field around the structural model. They are computationally less expensive and provide results for inviscid flows which are found to be in good agreement with Navier-Stokes solver for low values of non-dimensional frequency.

A brief study is made on the structural models of Brennan's insect flight mechanism and dipteran flight model with irrational non-linearity under external periodic forcing. A pure theoretical journey is undertaken into the realms of Lumped Vortex Method and Unsteady Vortex Lattice Method as flow solvers and their validity and limitations of application are assessed. The simulation of flow under Lumped Vortex Method is also studied for the observation of different kinds of vortex street patterns.

In the later parts, the effect of coupling of the Unsteady Vortex Lattice Method with Brennan's insect flight model and the non-linear aero-elastic model having pitch and plunge degrees of freedom is explored and the resulting dynamics are studied and analysed.

CONTENTS

LIST OF FIGURES

ABBREVIATIONS

FSI	Fluid Structure Interaction
CFD	Computational Fluid Dynamics
LVM	Lumped Vortex Method
VLM	Vortex Lattice Method
UVLM	Unsteady Vortex Lattice Method
HSPM	Hess-Smith Panel Method
MAV	Micro Aerial Vehicle
LCO	Limit Cycle Oscillation
DOF	Degree Of Freedom
FFT	Fast Fourier Transform

NOTATIONS

u	1. Non-dimensional vertical displacement in Brennan's insect flight model 2. Velocity in x direction
y	1. Dimensional vertical displacement in Brennan's insect flight model 2. Non-dimensional vertical displacement in dipteran flight model with irrational non-linearity
γ	Damping factor in Brennan's insect flight model
ζ	Damping coefficient in dipteran flight model with irrational non-linearity
ω_0	1. Natural frequency in Brennan's insect flight model 2. Natural frequency in dipteran flight model with irrational non-linearity
P	Dimensional forcing amplitude in Brennan's insect flight model
m	1. Mass of Brennan's insect flight model 2. Mass of airfoil in non-linear aero-elastic model having pitch and plunge DOF
ω	1. Dimensional frequency of external forcing in Brennan's insect flight model 2. Non-dimensional frequency of external forcing in dipteran flight model with irrational non-linearity
t	1. Dimensional time in Brennan's insect flight model 2. Dimensional time in non-linear aero-elastic model having pitch and plunge DOF
τ	Non-dimensional time in dipteran flight model with irrational non-linearity
f	1. Non-dimensional forcing amplitude in Brennan's insect flight model 2. Non-dimensional forcing amplitude in dipteran flight model with irrational non-linearity
Γ	Vortex strength
V_∞	Free stream velocity
w	Velocity in z direction

L	Lift
M	Moment
C_p	Coefficient of pressure
C_l	Coefficient of lift
C_m	Coefficient of moment
C	Panel length
c	Chord length
ρ	Density of air
dt	Time step size
S_α	First mass moment of inertia of airfoil in non-linear aero-elastic model having pitch and plunge DOF
I_α	Second mass moment of inertia of airfoil in non-linear aero-elastic model having pitch and plunge DOF
C_h	Damping co-efficient in plunge in non-linear aero-elastic model having pitch and plunge DOF
C_α	Damping co-efficient in pitch in non-linear aero-elastic model having pitch and plunge DOF
K_h	Linear spring stiffness in plunge in non-linear aero-elastic model having pitch and plunge DOF
K_α	Linear spring stiffness in pitch in non-linear aero-elastic model having pitch and plunge DOF
K_{h1}	Non-linear spring stiffness in plunge in non-linear aero-elastic model having pitch and plunge DOF
$K_{\alpha 1}$	Non-linear spring stiffness in pitch in non-linear aero-elastic model having pitch and plunge DOF
$L(t)$	Lift at any time step in non-linear aero-elastic model having pitch and plunge DOF
$F(t)$	External force at any time step in non-linear aero-elastic model having pitch and plunge DOF
$M(t)$	Moment at any time step in non-linear aero-elastic model having pitch and plunge DOF
U^*	Non-dimensional free stream velocity

CHAPTER ONE

SIMULATION OF UNCOUPLED STRUCTURAL MODEL

1.1 Introduction

To study any flight model we have to separately study structural response and flow dynamics. Our prime objective is to couple the structural model with a suitable flow model and therefore apparently, a separate study of a structural model may not have any significance. But without a study of such separate uncoupled model we cannot observe the change in behaviour due to intrusion of flow dynamics into the structural model. Basically, we cannot observe the effect of the flow part without a separate study of structure of the aerofoil or flat plate we are dealing with.

1.2 Choice of structural model

Since we want to study a model of an insect wing under influence of certain flow we have to consider the structure as a flat plate or thin aerofoil. There are some oscillatory models which may conform to insect wings. Some such models are:

- Brennan *et al.* modelled an insect flight motor which resembles the Duffing oscillator. But in Brennan's model the insect wing is considered as a flat plate.
- Again, Wiercigroch *et al.* have shown that the structural model for dipteran flight motor follows some irrational non-linearity.
- The previous two models are incorporated with single degree of freedom. If we want to incorporate two degrees of freedom in our structural model, we will follow a model having pitch and plunge degrees of freedom.

Analysis of the wing structure and modelling it is not our goal in this project. Therefore, we will briefly discuss about the established models only without going deeply into these.

1.2.1 Brennan's insect flight model

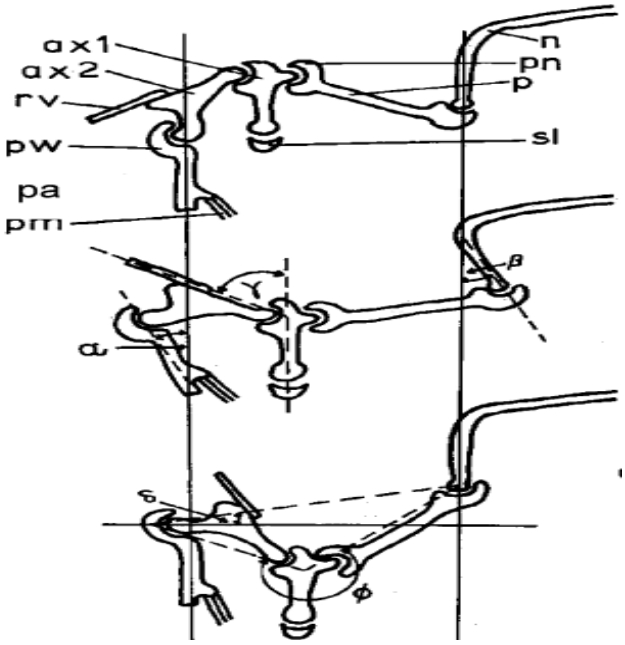

Fig. 1.1: Brief view of an insect

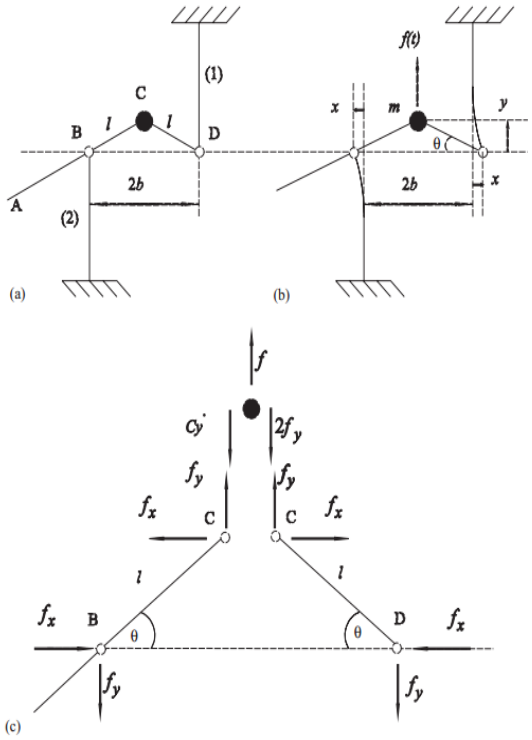

Fig. 1.2: Brennan's simplified model for insect wing

Ref. – 'The "Click" Mechanism in Dipteran Flight' by Brennan et al., Journal of Technical Biology (2003)

The governing equation for Brennan's oscillator model is:

$$\ddot{u} + \gamma\omega_0\dot{u} - \frac{\omega_0^2}{2}u(1-u^2) = \frac{P}{mL}\cos(\omega t) \qquad 1.1$$

Where, $u = y/L$ is non-dimensional displacement

$\omega_o{}^2 = \frac{4k}{m}\left(1 - \frac{b}{l}\right)$

γ = damping factor

$L = \sqrt{2\left(1 - \frac{b}{l}\right) / \left(\frac{b}{l}\right)^3}$

m = mass

$P/mL = f$ is non-dimensional forcing amplitude.

We can clearly observe that the equation given by Brennan *et al.* is nothing but a Duffing's equation. Therefore, an insect wing of a dipteran flight motor can be designed as a Duffing oscillator.

1.2.2 Dipteran flight model with irrational non-linearity

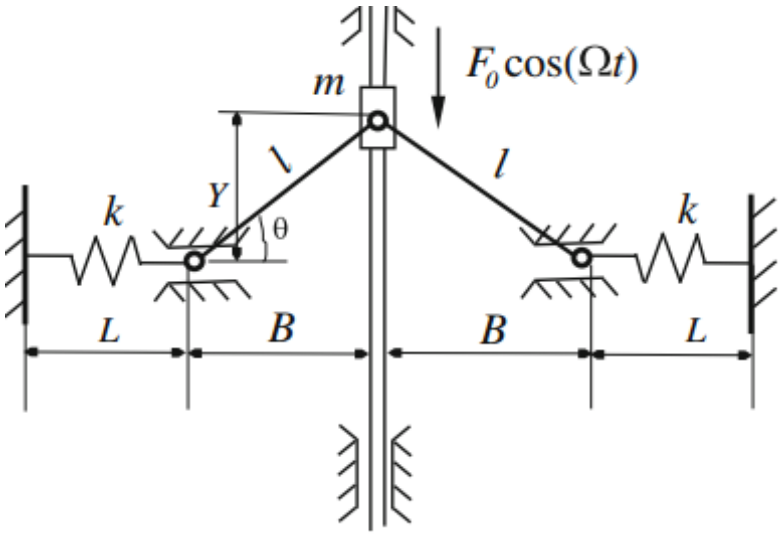

Fig. 1.3: Proposed dipteran flight model (analogous to the bar-spring system)

Ref. – 'A Novel Model of Dipteran Flight Mechanism' by Weircigroch et al., International Journal for Dynamic Control (2013)

The governing equation for model with irrational non-linearity is:

$$\ddot{y} + 2\zeta\dot{y} - \omega_0^2 y\left(1 - \frac{b}{\sqrt{1-y^2}}\right) = f\sin(\omega\tau) \qquad 1.2$$

Where, ζ = damping coefficient

$\tau = \omega_0 t$ is non-dimensional time

f = non-dimensional forcing

$y = Y/l$ is non-dimensional displacement

$b=B/l$

Now using some relevant parameter values we will simulate the structural models using structural solvers and observe the dynamics i.e. time history and phase portraits. Separate diagrams for dynamics of the structural solver for both the models will be given by simulating the solver for different forcing amplitude value. Hence we can get the change observed due to increasing forcing amplitude in the structural dynamics system.

1.3 Simulation results for uncoupled structural solver

We are showing results of structural simulation in form of time history of displacement and phase space diagram for both Brennan's model and Wiercigroch's model.

1.3.1 Brennan's insect flight model

Some simulated results are shown for changing non-dimensional amplitude value (f), other parameters being unchanged.

1.3.1.1 Time history of displacement

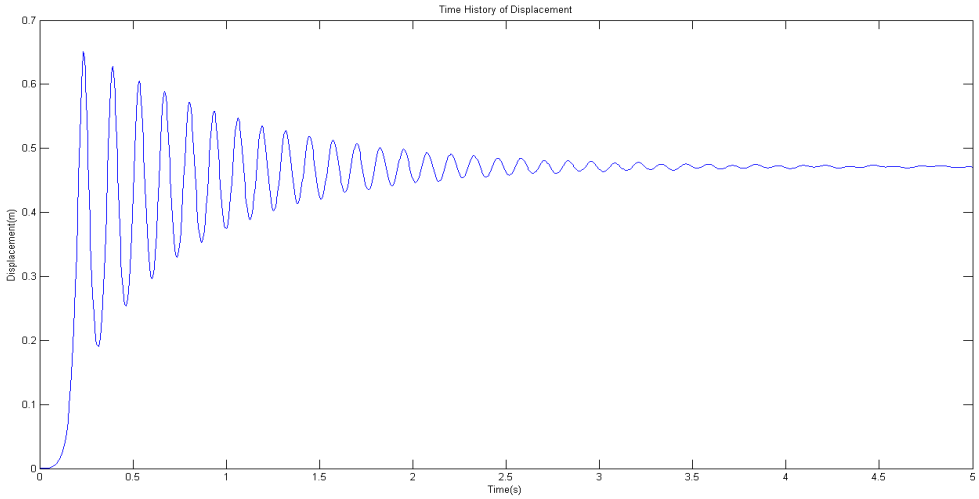

(a) f = 5

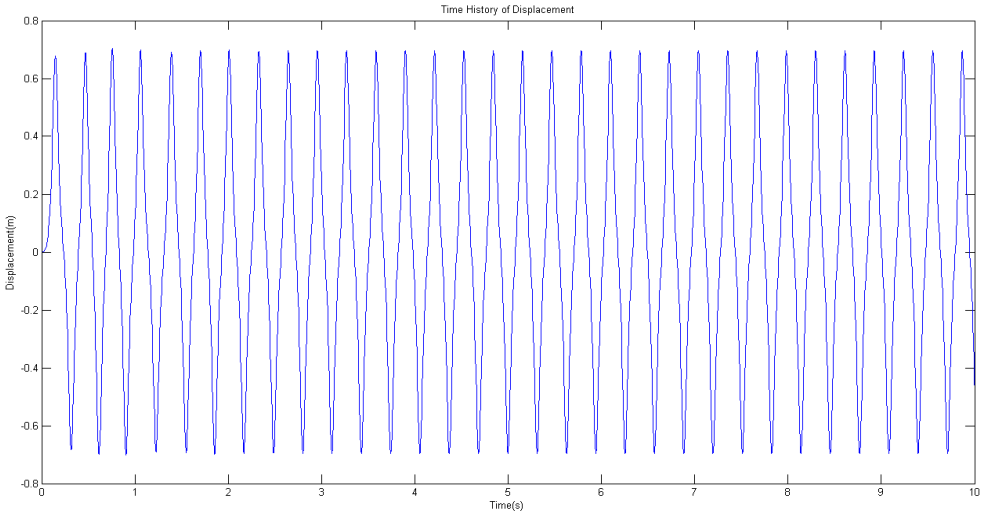

(b) f = 100

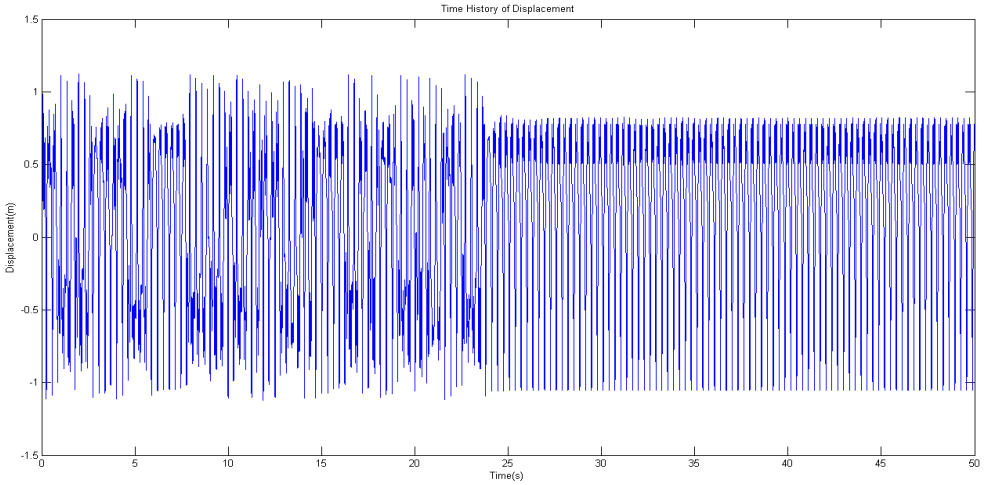

(c) f = 2000

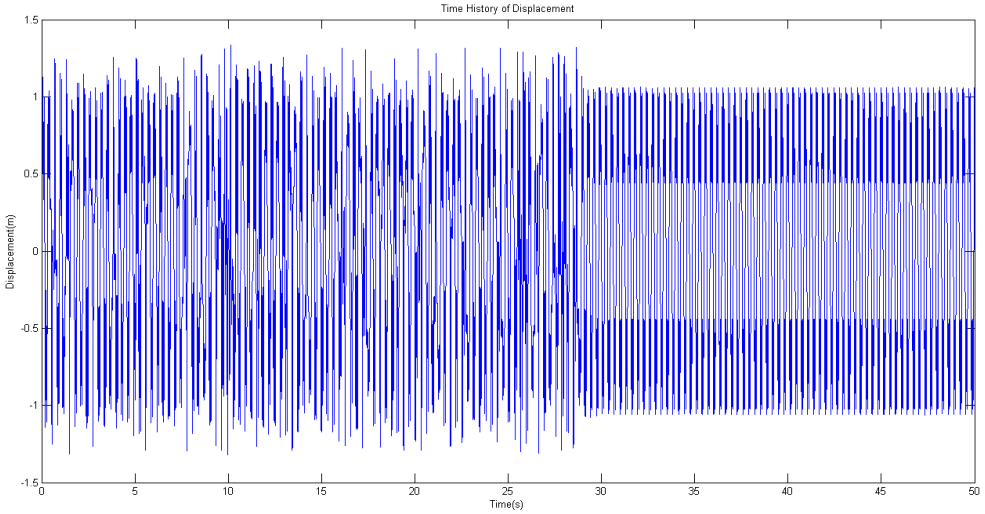

(d) f = 4000

Fig.1.4: (a), (b), (c), (d) - Time history of displacement for increasing f value

We can clearly observe for lower f value the damping is predominant and slowly the extent of oscillation decreases to a very small value and this small value is non-zero since there is some finite external forcing value. With increase in f value we can observe that the initial portion of the plot is having some transitional chaos and after a certain time which becomes periodic and this periodicity is also due to external forcing.

1.3.1.2 Phase space diagram

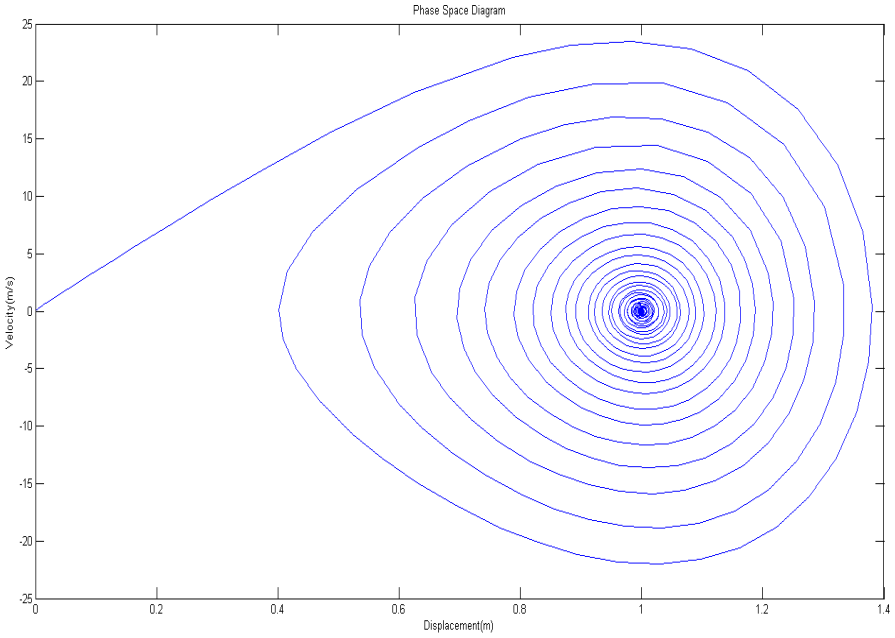

(a) f = 5

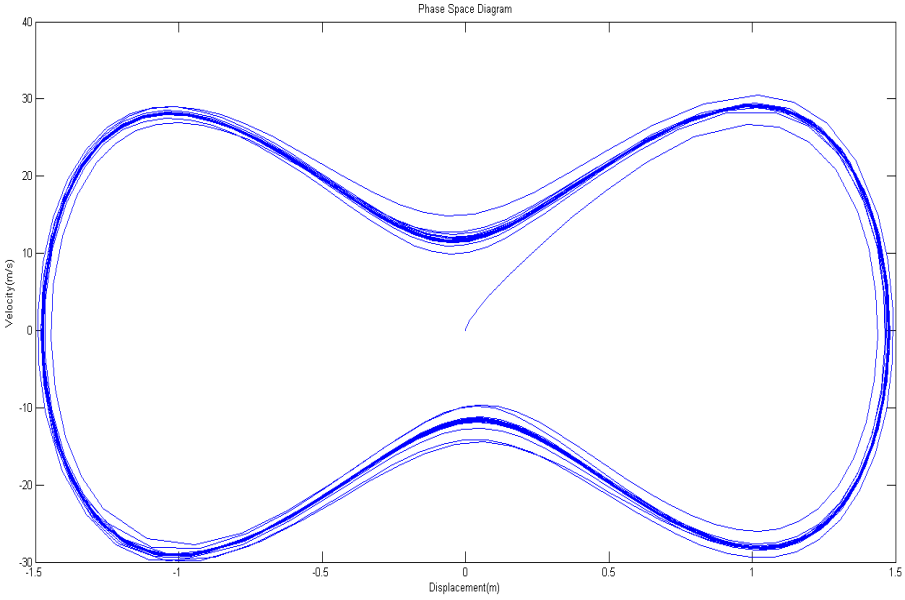

(b) f = 100

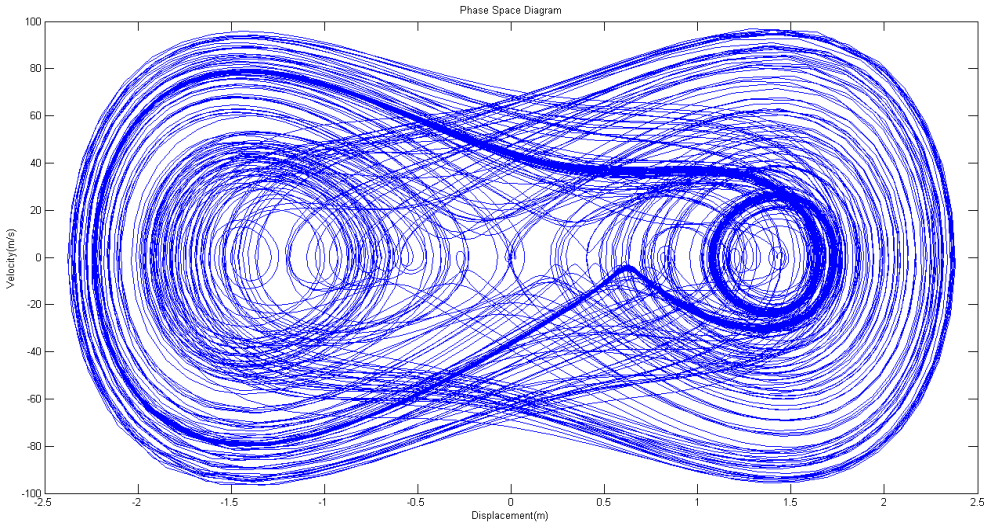

(c) f = 2000

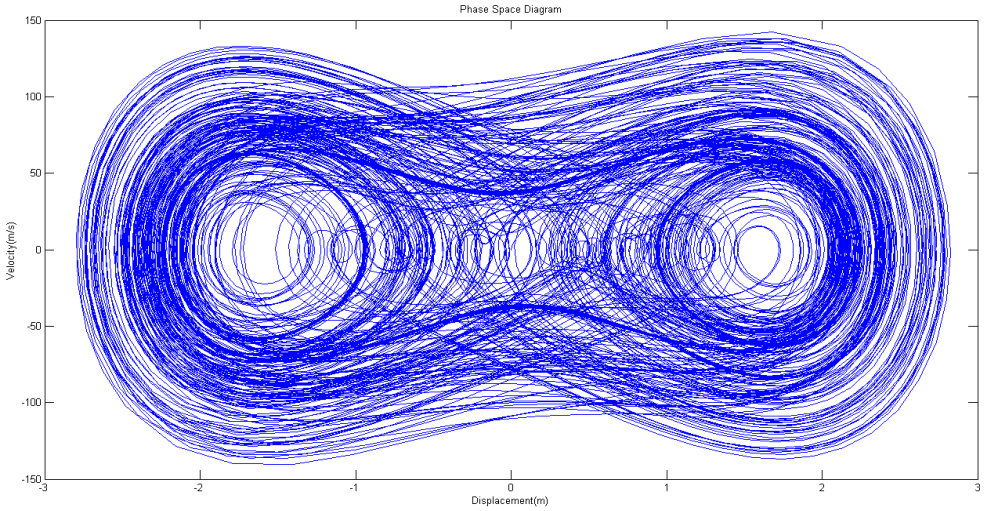

(d) f = 4000

Fig. 1.5: (a), (b), (c), (d) - Phase space diagram for increasing f value

We can observe that for very low forcing amplitude the phase space diagram looks like a single well and the curve is slowly converging to a single point. For higher value of *f,* we can see that the oscillation takes place between two wells. Due to the transitional part the diagrams look like chaotic ones.

1.3.2 Dipteran flight model with irrational non-linearity

Some simulated results are shown for changing non-dimensional amplitude value (*f*), other parameters being unchanged.

1.3.2.1 Time history of displacement

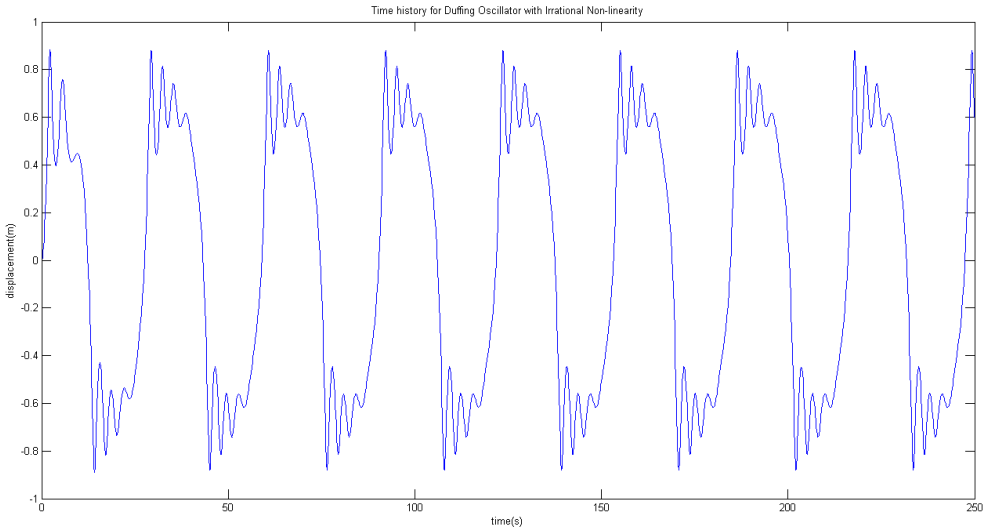

(a) $f = 0.125$

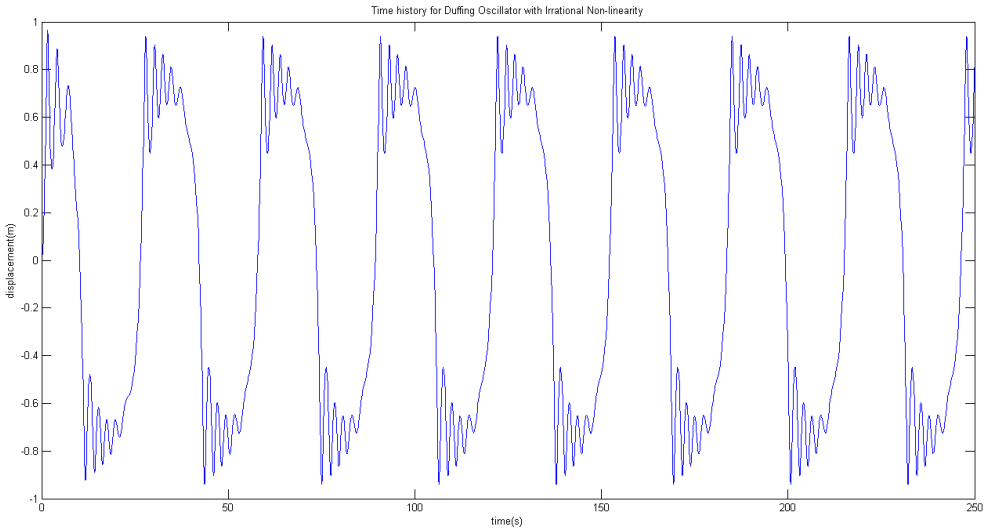

(b) $f = 0.25$

Fig. 1.6: (a), (b) - Time history of displacement for increasing *f* value

1.3.2.2 Phase Space Diagram

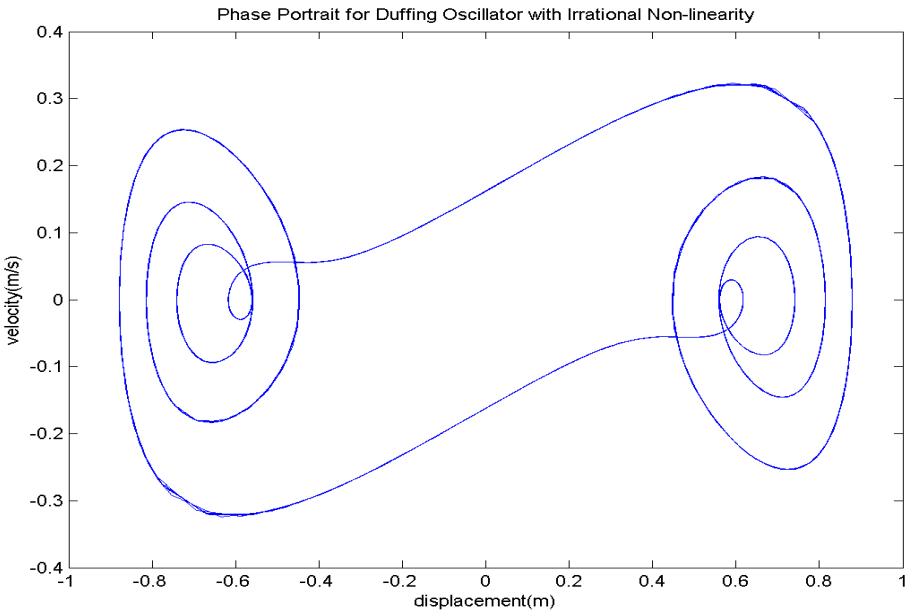

(a) f = 0.125

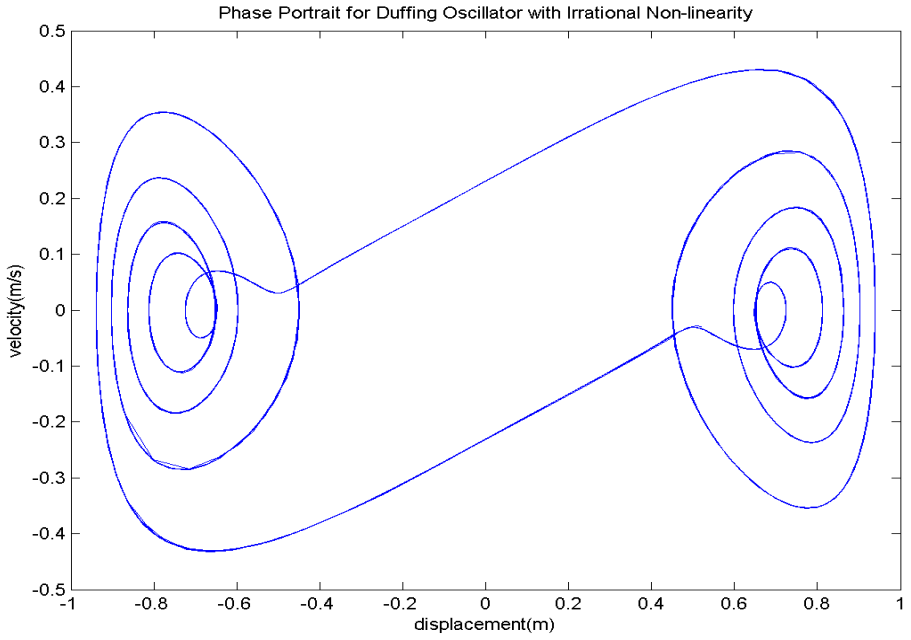

(b) f = 0.25

Fig. 1.7: (a), (b) - Phase space diagram (excluding transitional part) for increasing f value

In the time history of displacement, we can observe some kinks at the peaks of the curve. With increase in the forcing amplitude *f* the number of such irregular kinks increases. After certain value of *f*, the structural solver fails. Again in the phase space diagram for both the values of *f*, the diagrams show two well oscillation. To have a clear view of such oscillation we have omitted the transitional part. For higher value of *f*, each well seems to be more spiral one.

Here we have discussed about only single degree of freedom (SDOF) models. Among these two models we will use only the Brennan's model for coupling purpose in our main FSI problem. The other model of two degrees of freedom is not discussed here and it will be discussed in the coupling part itself. So our main structural models are Brennan's model for flat plate and the two degree of freedom model for thin aerofoil.

CHAPTER TWO

LUMPED VORTEX METHOD AS FLOW SOLVER

2.1 Introduction

In this project we are studying about the fluid structure interaction. Fluid structure interactions are a crucial consideration in the design of many engineering systems. In particular, the analysis of problems of biomechanical systems, micromechanical devices, the optimization and control of brake systems, aircraft wings, turbine blades, analysis of large arteries and artificial heart valves, bridges etc. As a consequence, the development of more effective methods for the solution of FSI problems is important.

Different strategies have been proposed to solve FSI problems and the selection of the most effective approach strongly depends on the characteristics of problem to be analyzed. Specifically, the mathematical model employed in the description of the fluid behavior plays a decisive role in the selection of the most suited solution procedure.

The main approaches employed in the solution of FSI problems are the simultaneous (direct) and the partitioned (iterative) solution procedures. In the simultaneous solution procedure, the fluid and solid equations are established and solved together. In a partitioned procedure, each field (fluid and solid) is solved separately and solution variables (forces, or velocities and displacements at the interface) are passed iteratively from one field to the other until convergence is achieved (for each time or load step). It should be pointed out that a full coupling between the media is achieved by using any of the above-mentioned procedures. Usually, partitioned procedures are preferred when the interaction between the fluid and the structure is weak and the simultaneous solution procedure is employed when there is a strong coupling. In this section, the equations that govern the behavior of fluids modeled using the lumped vortex method and general structures are considered together with the conditions that must be satisfied at the fluid-structure interfaces.

2.2 Lumped Vortex Method

The Lumped Vortex Method (LVM) provides a numerical (approximated) solution for the fundamental equation of the thin-airfoil problem. In Lumped Vortex Method, our elementary flow is vortex flow. LVM is used in the analysis of lifting flow over the thin airfoil. LVM is numerically very less costly and less time consuming method. Also it gives very accurate results in the case of incompressible and inviscid flow over airfoil. So LVM is very preferable method than CFD methods in above case. LVM allows to compute the airfoil lift and moment characteristics and, C_p and C_m distribution across the mean line.

2.3 Methodology of LVM

2.3.1 Assumptions

1. Here our airfoil body is flat plate.
2. Flow over the flat plate is incompressible and inviscid flow.
3. There is no flow separation at the trailing edge of flat plate.

2.3.2 Discretization of geometry

First step of LVM method is to divide the airfoil into *N* numbers of small straight elements which are called panels. So airfoil will become a series of the *N* numbers of panels. This discretization of geometry does have effect on the solution in many ways like in how many numbers of panels we are dividing the airfoil, length of panels, panel distribution, vortex strength distribution on the panels etc.

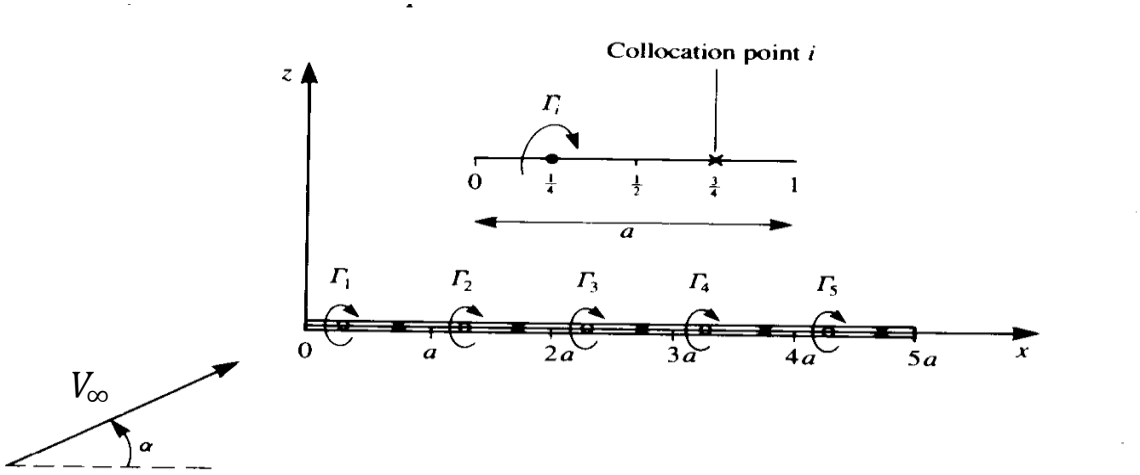

Fig. 2.1: Discretization of geometry, selection of control and collocation points

2.3.3 Selection of control points and collocation points

Once the discretization of airfoil is performed, some geometrical data must be computed for each panel *j*, namely: unit tangent and normal vectors, the coordinates of the control and the collocation points, and the panel length (C_j). This information can be obtained for each panel as follows:

$$\Delta x = x_{j+1} - x_j \quad , \quad \Delta z = z_{j+1} - z_j$$

Where (x_j, z_j) and (x_{j+1}, z_{j+1}) are the two end points of the j^{th} panel.

So the length of j^{th} panel is $C_j = \sqrt{\Delta x^2 + \Delta z^2}$

Normal vector: $n_j = \left(\frac{\Delta z}{C_j}, \frac{\Delta x}{C_j}\right)$ and, Tangential vector: $t_j = (\frac{\Delta x}{C_j}, \frac{\Delta z}{C_j})$

Here control points are the points where vortex element is considered and collocation points are the points where boundary conditions are applied.

In LVM at each panel, the point vortex is located at the quarter panel chord and the collocation point is at ¾th of the panel chord. It is easy to demonstrate that this choice allows satisfying the Kutta condition in an implicit manner.

2.3.4 The system of equations for the vortex strengths

In this method we take vortex element singularities at the ¼th of the panel length and try to find out the strength of these vortex singularities for each panel in such way that the airfoil body becomes a streamline of the flow. For that we have to satisfy two boundary conditions.

1. At each collocation point the normal velocity induced due to vortex element and free stream must be set to zero. This will give us *N* linear equations for *N* panels.

$$[V_\infty(cos\alpha, sin\alpha) + \sum_{j=1}^{N} \Gamma_j \left(u_{ij}, w_{ij}\right)]. (n_{ix}, n_{iz}) = 0 \qquad 2.1$$

Here *i = 1, 2, 3,……,N*.

Where (u_{ij}, w_{ij}) is the velocity induced at the i^{th} collocation point by a vortex of unit intensity located at the quarter chord point of a panel *j* which are called influence coefficients. Γ_j are the unknown vortex strengths.

The induced velocities can be calculated as:

$$u_{ij} = \frac{1}{2*\pi} * \frac{z_i - z_j}{r^2} \quad , \quad w_{ij} = -\frac{1}{2*\pi} * \frac{(x_i - x_j)}{r^2} \tag{2.2}$$

Where $r^2 = \left(x_i - x_j\right)^2 + \left(z_i - z_j\right)^2$ and, (x_i, z_i) is the position of the collocation point of the i^{th} panel and (x_j, z_j) is the position of vortex element of j^{th} panel.

Equation 2.1 can be rearranged by moving free velocity term to RHS side,

$$\sum_{j=1}^{N} \Gamma_j \left(u_{ij}, w_{ij}\right).(n_{ix}, n_{iz}) = -V_\infty(cos\alpha, sin\alpha)\ (n_{ix}, n_{iz}) \tag{2.3}$$

In this equation influence coefficients can be given as below:

$$A_{ij} = u_{ij} * n_{ix} + w_{ij} * n_{iz} \tag{2.4}$$

The term on RHS in equation 2.3 which is a function of geometry and flight condition can also be written as

$$RHS_i = -V_\infty * (cos \propto . n_{ix}, sin \propto . n_{iz}) \tag{2.5}$$

2. Second boundary condition is Kelvin's circulation theorem. According to this theorem total circulation of the airfoil vortex strengths is equal to the circulation induced due to wake vortices at the downstream of the trailing edge of the airfoil.

   So, $\sum_{J=1}^{N} \Gamma_J =$ total circulation of wake vortices

   From this,

$$A_{i+1j} = 1 \tag{2.6}$$

Where *j = 1,2,3,…..,N,* and,

$$RHS_{i+1} = \sum_{J=1}^{N} \Gamma_j \tag{2.7}$$

So now there are (*N+1*) equations and *N* unknowns. Take any (*N-1*) equation from first boundary condition and one equation from second boundary condition and make matrix of it which can be written as,

$$A.\Gamma = RHS \tag{2.8}$$

By solving this matrix, we will get the value of vortex strengths for all panels which satisfy the streamline flow condition.

2.3.5 Lift and moment calculations

Once the *Γ* distribution is known, the panel lift and pressure distribution can be computed by the Kutta–Joukowski theorem.
So the lift and pressure generated on i^{th} panel is given by,

$$\Delta L_i = \rho * V_\infty * \Gamma_i \tag{2.9}$$

$$\Delta P_i = \rho * V_\infty * \frac{\Gamma_i}{c_i} \tag{2.10}$$

Where c_i is the length of the i^{th}panel.
So total lift and moment is given by,

$$L = \sum_{i=1}^{N} \Delta L_i \tag{2.11}$$

$$M = -\sum_{i=1}^{N} \Delta L_i * (x_{ci} - x_{ref}) \tag{2.12}$$

Where x_{ci} is the collocation point of the panel i^{th} and x_{ref} is the reference point adopted for computing the moment.

So lift and moment coefficients can be calculated by following equations,

$$C_l = \frac{L}{\left(\frac{1}{2}\right) * \rho * V_\infty^2 * c} \tag{2.13}$$

$$C_m = \frac{M}{\left(\frac{1}{2}\right) * \rho * V_\infty^2 * c^2} \tag{2.14}$$

Where *c* is the chord length.

2.4 Validation of LVM

Before using this method for analysis one should validate it whether this method gives accurate result or not. For that MATLAB code have been written for LVM and plotted it with Navier-Stokes method results and compared it.

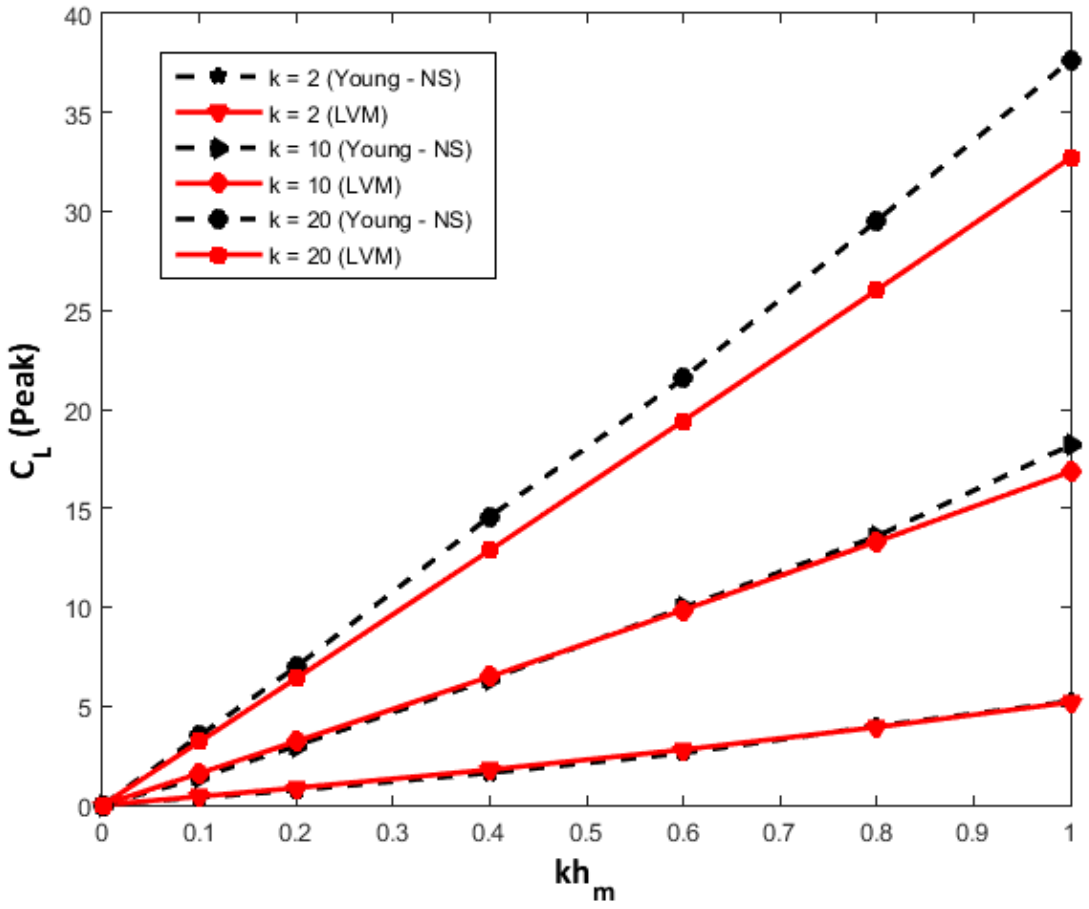

Fig. 2.2: Validation of LVM with Navier-Stokes method

Here in the graph the black lines represent Navier-Stokes results and red lines represent LVM results. For the lower value of *k*, both results match with each other.

But for the higher value of *k* there is somewhat difference in the results. This is due to separation of flow at the trailing edge for higher value of *k*. Navier-Stokes method takes this effect into consideration. In LVM, it is assumed that flow is attached to the airfoil surface and there is no flow separation. Because of this assumption there is difference in the results. But still LVM gives satisfactory results. So LVM is very appropriate method for this analysis.

2.5 Trailing edge vortex pattern

After coding the LVM in MATLAB, some wake vortex patterns were obtained at the downstream of trailing edge for the case of pure plunging.

In the case of pure plunging of flat plate, flow dynamics have been considered to be sinusoidal. So the displacement of the flat plate is given by,

$$Y = Asinwt \tag{2.15}$$

Where *A* = amplitude of plunging

w = frequency of plunging in $\frac{rad}{s}$

t = time

Non-dimensional form of equation 2.15 can be obtained by putting,

$$h = \frac{A}{c}, \qquad k = w * \frac{b}{V_\infty} \qquad \text{and} \qquad \tau = t * \frac{V_\infty}{b} \tag{2.16}$$

Here, *c* = chord length

V_∞ = Free stream velocity and *b* = *c/2*.

So non-dimensional equation is,

$$Y = (h * c)sink\tau \tag{2.17}$$

$$\bar{y} = hsink\tau \tag{2.18}$$

This is the governing equation for plunging in this case.

2.5.1 Solution and plotting

By using above equation and LVM flow solver in the MATLAB coding, some wake vortex patterns were plotted for the different value of *kh*.

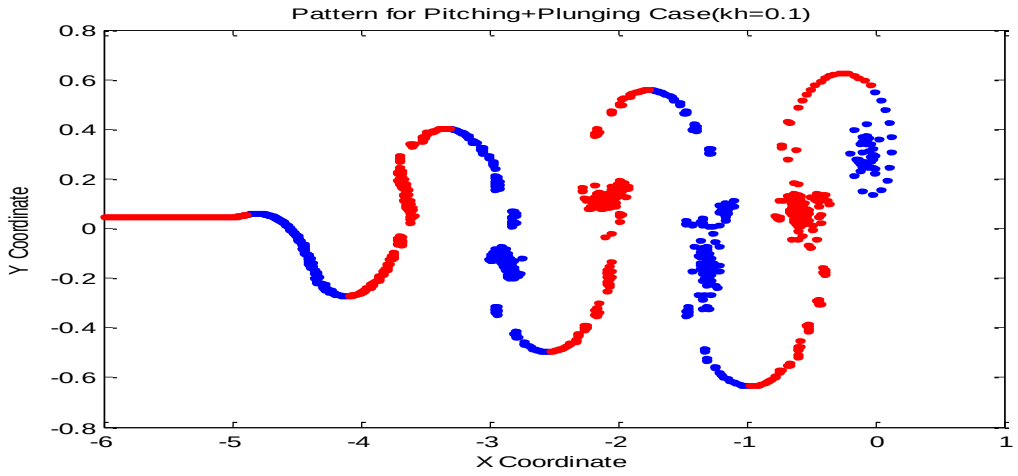
Pattern for Pitching+Plunging Case(kh=0.1)
Y Coordinate
X Coordinate
0.8
0.6
0.4
0.2
0
-0.2
-0.4
-0.6
-0.8
-6
-5
-4
-3
-2
-1
0
1

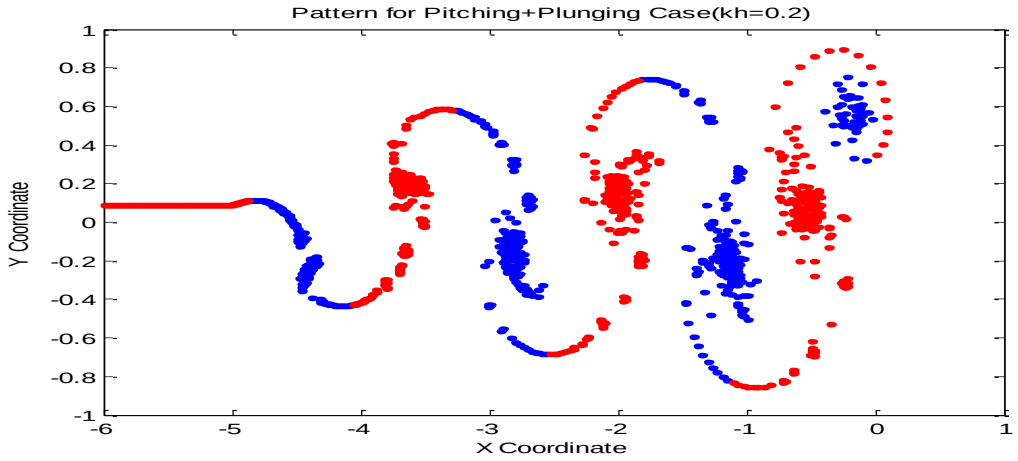
Pattern for Pitching+Plunging Case(kh=0.2)
Y Coordinate
X Coordinate
1
0.8
0.6
0.4
0.2
0
-0.2
-0.4
-0.6
-0.8
-1
-6
-5
-4
-3
-2
-1
0
1

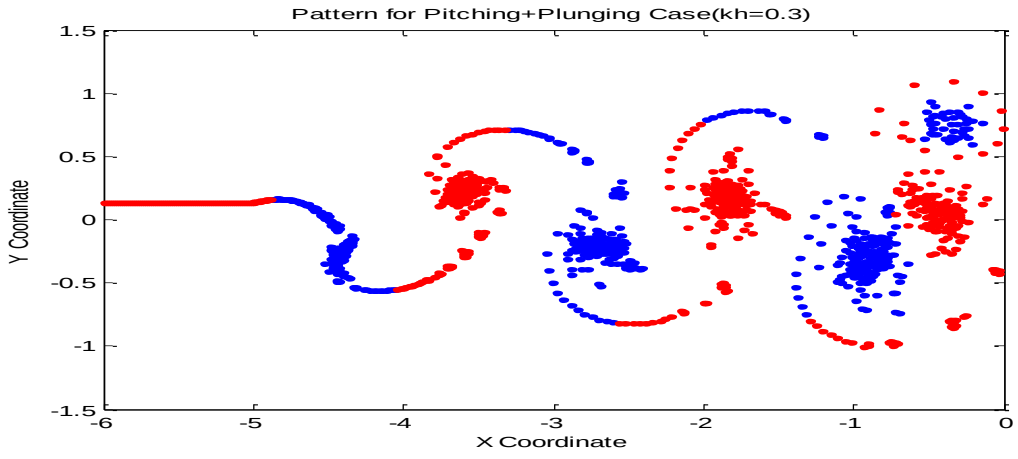
Pattern for Pitching+Plunging Case(kh=0.3)
Y Coordinate
X Coordinate
1.5
1
0.5
0
-0.5
-1
-1.5
-6
-5
-4
-3
-2
-1
0

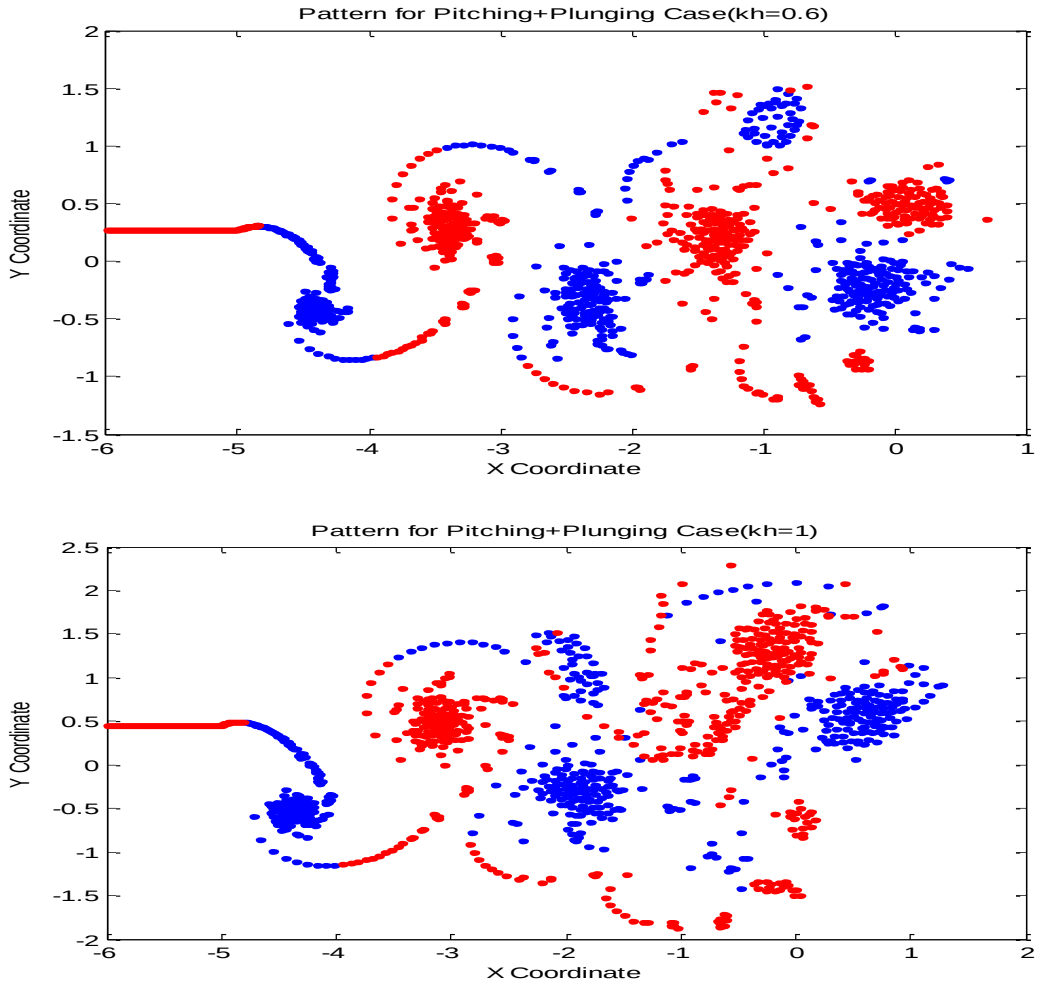

Fig. 2.3: Y-coordinate vs X-coordinate plot for pure plunging case using LVM

There are two types of wake vortex pattern:

1) Kármán Vortex Pattern
2) Anti-Kármán Vortex Pattern

From the graph, it can be seen that for the *kh* value of 0.1, 0.2 and 0.3 anti-Kármán patterns are there and for *kh* value of 0.6 and 1 deflected patterns are there.

CHAPTER THREE

UNSTEADY VORTEX LATTICE METHOD AS FLOW SOLVER

3.1 Introduction

The utility of the panel methods in analysing the dynamics of aerofoils is already discussed in the previous chapter. Unsteady Vortex Lattice Method is another approach for such analysis other than LVM. The difference of vortex lattice method with LVM is in the structural model used and also in the elementary flows considered. LVM assumes a flat plate and vortex distribution forms the model. In VLM the aerofoil geometry is realized by applying vortex and source flow. The Unsteady Vortex Lattice Method is also known as Hess-Smith Panel Method (HSPM) after Hess and Smith, who developed it in 1966 while working at Douglas Aircraft.

3.2 Difference between steady and unsteady VLM

In case of inviscid and incompressible flow, like LVM, VLM is also an effective method to analyse lifting flow over aerofoil, more preferable to time-consuming CFD methods like LVM. The difference of the unsteady dynamics with the steady is that the aerofoil sheds a vortex at its trailing edge as it moves and lets this vortex change or affect its dynamics.

3.3 Methodology of UVLM

3.3.1 Assumptions

1. The flow is over a two dimensional aerofoil section.
2. The flow is incompressible and inviscid.
3. There is no flow separation at trailing edge.

3.3.2 Discretization of geometry

Similar to LVM we divide the periphery into *N* number of panels and the panels are numbered clockwise starting from the trailing edge.

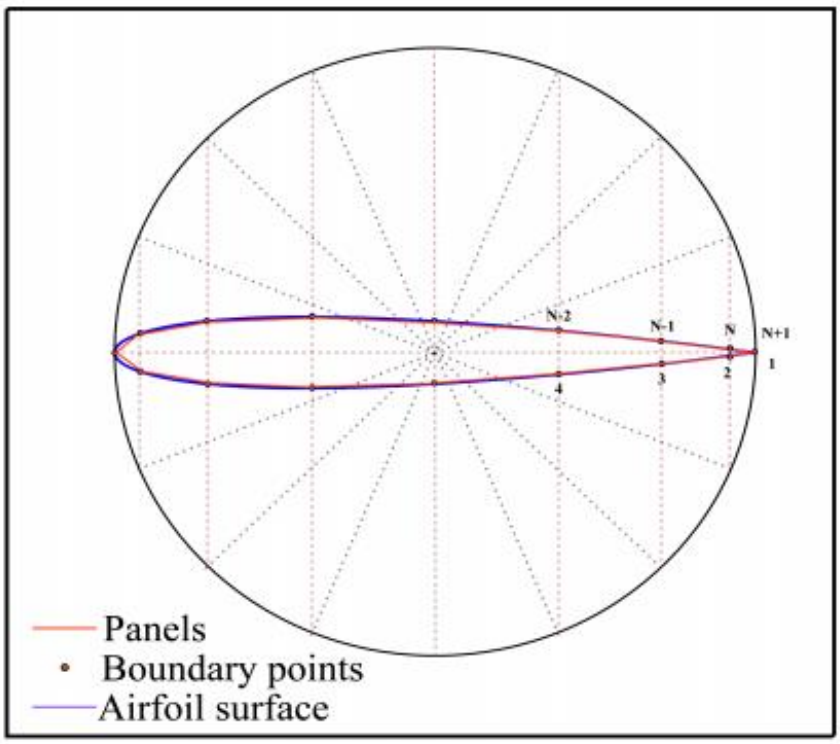

Fig. 3.1: Determination of boundary points

3.3.3 Selection of control points

The control points and collocation points reside at the centre of each panel and the aerodynamic centre is assumed to be at $1/4^{th}$ of the chord length from leading edge.

3.3.4 Model of the flow

In this flow model, the elementary flows are source flow and vortex flow. A uniform vortex sheet all over the aerofoil and a uniform source sheet on each panel is considered to model the aerofoil surface streamline.

Let there be uniform vorticity strength (τ) all over the panels and different source strength distribution (q_j) on each panel (j) for each time step k. Here the midpoints of the panels are considered as the control points.

3.3.5 Steps followed

3.3.5.1 Calculation of source and vortex strengths

For each time step these source and vortex strengths are found out by application of boundary conditions. The two sets of boundary conditions used are:

Condition 1: No normal flow

Here, surface of the body is streamline of the flow. Hence, the resultant velocity (summation of velocity induced due to sources, bound vortices, shed vortex, wake vortices and flow velocity) at each control points in the direction normal to the surface is set to be zero. Hence,

$$(V_i^n)_k = \sum_{j=1}^{N} A_{ij}^n q_j + \tau \sum_{j=1}^{N} B_{ij}^n + \left(\vec{V}_{stream}.\vec{n}_i\right)_k + (\tau_w)_k \left(B_{i,n+1}^n\right)_k + \sum_{m=1}^{N}\left(C_{i,n}^n\right)_k (\Gamma_{m-1} - \Gamma_m) = 0 \quad (3.1)$$

Where, *i = 1,2,3,…,N.*

The influence coefficients on i^{th} panel due to all panel sources is *A*, due to bound vortices is *B*, due to wake vortices is *C*.

$$A_{ij}^n = \frac{1}{(2*\Pi)}\left[sin\left(\Theta_i - \Theta_j\right) ln\left(\frac{r_{i,j+1}}{r_{i,j}}\right) + cos\left(\Theta_i - \Theta_j\right)\beta_{i,j}\right] \qquad i \neq j$$

$$A_{ij}^n = \frac{1}{2} \qquad i = j$$

$$A_{ij}^t = \frac{1}{(2*\Pi)}\left[-cos\left(\Theta_i - \Theta_j\right) ln\left(\frac{r_{i,j+1}}{r_{i,j}}\right) + sin\left(\Theta_i - \Theta_j\right)\beta_{i,j}\right] \qquad i \neq j$$

$$A_{ij}^t = 0 \qquad i = j \quad (3.2)$$

From source and vortex strength expressions, we can write,

$$B_{ij}^n = -A_{ij}^t \,,\; B_{ij}^t = A_{ij}^n \quad (3.3)$$

Kelvin's circulation theorem:

As the total circulation in the flow field must be preserved, vortices are shed to balance any change in the circulation (*Γ*) on the aerofoil surface. So,

$$\Delta_k(\tau_w)_k = \Gamma_{k-1} - \Gamma_k = l(\tau_{k-1} - \tau_k) \quad (3.4)$$

After putting this value in earlier equation and solving it we can get source strength (q_j) in terms of vortex strength (τ).

Condition 2: Unsteady Bernoulli's theorem

In the case of unsteady flow, the Kutta condition must include the rate of change of velocity potential, i.e.,

$$[(V^t)_1]_k^2 - [(V^t)_N]_k^2 = 2\left[\frac{\partial(\emptyset_N - \emptyset_1)}{\partial t}\right]_k = 2\left[\frac{\partial(\Gamma)}{\partial t}\right]_k \quad 3.5$$

Using backward finite difference method,

$$[(V^t)_1]_k^2 - [(V^t)_N]_k^2 = 2\frac{(\Gamma_k - \Gamma_{k-1})}{t_k - t_{k-1}} = 2l\frac{(\tau_k - \tau_{k-1})}{t_k - t_{k-1}} \quad 3.6$$

Now solving these equations, we can get the value of τ and from that source strength q_j.

3.3.5.2 Effect on wake panel

From τ and q_j we get the velocities at the midpoints of the wake panels, u_w and v_w can be written as,

$$u_w = \sum_{j=1}^{N} A_{wj}^n q_j + \tau \sum_{j=1}^{N} B_{wj}^n + \left(\vec{V}_{stream}.\vec{n}_w\right)_k + \sum_{m=1}^{N}\left(C_{w,n}^n\right)_k(\Gamma_{m-1} - \Gamma_m) \quad 3.7$$

$$v_w = \sum_{j=1}^{N} A_{wj}^t q_j + \tau \sum_{j=1}^{N} B_{wj}^t + \left(\vec{V}_{stream}.\vec{n}_w\right)_k + \sum_{m=1}^{N}\left(C_{w,t}^t\right)_k(\Gamma_{m-1} - \Gamma_m) \quad 3.8$$

Now, update $\theta_k = tan^{-1}\left(\frac{v_w}{u_w}\right)$ and $\Delta_k = (t_k - t_{k-1})\sqrt{(u_w)_k^2 + (v_w)_k^2}$.

3.3.5.3 Calculation of lift and moment

In unsteady flow the pressure coefficient is dependent on the rate of change of velocity potential. So, from Bernoulli's equation, we may write,

$$C_p = \frac{p - p_\infty}{\frac{1}{2} * \rho V_\infty^2} \quad 3.9$$

Where, C_p = pressure coefficient.

Using backward finite difference method again, the pressure coefficient at the i^{th} control point at time step k,

$$[(C_p)_i]_k = \frac{[(V_{stream})_i]_k^2}{V_\infty^2} - \frac{[(V_t)_i]_k^2}{V_\infty^2} - \frac{2}{V_\infty^2}\frac{[(\phi_i)_k - (\phi_i)_{k-1}]}{(t_k - t_{k-1})} \quad 3.10$$

Where the terms are

- The tangential velocity component on the i^{th} panel

$$(V_i^t)_k = \sum_{j=1}^{N} A_{ij}^t q_j + \tau_k \sum_{j=1}^{N} B_{ij}^t + \left(\vec{V}_{stream}.\vec{n}_i\right)_k + (\tau_w)_k \left(B_{i,n+1}^t\right)_k + \sum_{m=1}^{N}\left(C_{i,n}^t\right)_k (\Gamma_{m-1} - \Gamma_m) \quad 3.11$$

- The velocity potential is evaluated integrating the velocity field
  - From upstream at infinity to the aerofoil leading edge.
  - Along aerofoil surface from leading edge to each panel control point.

For this purpose we choose an arbitrary straight line from leading edge extending upstream to the infinity parallel to V_∞. This line is divided into z panels with element lengths near the leading edge comparable to the panel sizes near the leading edge along the aerofoil and it is progressively increased as the induced velocity decays inversely with distance from the leading edge.

Here the tangential velocities at the control point of each front panel is,

$$[(V_\emptyset^t)_f]_k = \sum_{j=1}^{N} A_{fj}^t q_j + \tau_k \sum_{j=1}^{N} B_{fj}^t + \left(\vec{V}_{stream}.\vec{n}_i\right)_k + (\tau_w)_k \left(B_{f,n+1}^t\right)_k + \sum_{m=1}^{N}\left(C_{f,n}^t\right)_k (\Gamma_{m-1} - \Gamma_m) \quad 3.12$$

Velocity potential at the leading edge,

$$(\phi_{l.e})_k = \sum_{f=1}^{z} ((V_\emptyset^t)_f)_k \sqrt{\left(x_{f+1} - x_f\right)^2 + \left(y_{f+1} - y_f\right)^2} \quad 3.13$$

Velocity potential at i^{th} boundary point on the aerofoil is:

$$(\phi_{node\ i})_k$$

$$= (\phi_{l.e})_k + \sum_{j=i_{l.e}}^{i-1} [(V_\emptyset^t)_j]_k \sqrt{\left(x_{j+1} - x_j\right)^2 + \left(y_{j+1} - y_j\right)^2} \quad i_{l.e} \le i \le N$$

$$= (\phi_{l.e})_k - \sum_{j=1}^{i_{l.e}-1} [(V_\emptyset^t)_j]_k \sqrt{\left(x_{j+1} - x_j\right)^2 + \left(y_{j+1} - y_j\right)^2} \quad 1 \le i < i_{l.e} \quad 3.14$$

Hence velocity potential at i^{th} panel control point is

$$(\phi_i)_k = \frac{1}{2}[(\phi_{node\ i})_k + (\phi_{node\ i+1})_k] \quad 3.15$$

Now we can find C_p for each panel at a time step from the earlier equation knowing the value of ϕ. Hence again we can find out the total lift and drag for all the panels from which we can calculate C_d, C_l and C_m by taking suitable components with respect to the global axes system.

$$Lift = \frac{1}{2}\rho V_\infty^2 (C_l)_k \quad 3.16$$

$$Moment = \frac{1}{2} V_\infty^2 (C_m)_k \quad 3.17$$

Now we can add this lift and moment with the force and moment in the structural equations of motion in our structural models.

For wake vortices, the velocity components along x and y direction due to the source distribution, bound vorticity distribution, free stream velocity, shed vortex panel and wake vortices can be written as

$$(u_h)_k = \sum_{j=1}^{N}(A_{hj}^x)_k\, q_j + \tau_k \sum_{j=1}^{N}(B_{hj}^x)_k + \left(\vec{V}_\infty.\vec{i}\right)_k + (\tau_w)_k \left(B_{h,n+1}^x\right)_k + \sum_{m=1,m\neq h}^{N}\left(C_{h,n}^t\right)_k(\Gamma_{m-1} - \Gamma_m) \quad 3.18$$

$$(v_h)_k = \sum_{j=1}^{N}(A_{hj}^y)_k\, q_j + \tau_k \sum_{j=1}^{N}(B_{hj}^y)_k + \left(\vec{V}_\infty.\vec{j}\right)_k + (\tau_w)_k \left(B_{h,n+1}^y\right)_k + \sum_{m=1,m\neq h}^{N}\left(C_{h,n}^t\right)_k(\Gamma_{m-1} - \Gamma_m) \quad 3.19$$

Hence we can find out the vortex pattern of the wake vortex as well as core vortices by having the time displacement relationship.

3.4 Validation of UVLM

Before the UVLM flow solver could be used for coupling of flow with the structural model, the UVLM code needs to be verified whether it provides acceptable results depicting the true physics of the fluid flow. The validation of the UVLM MATLAB code is done with the more accurate Navier-Stokes solver as done before in case of LVM.

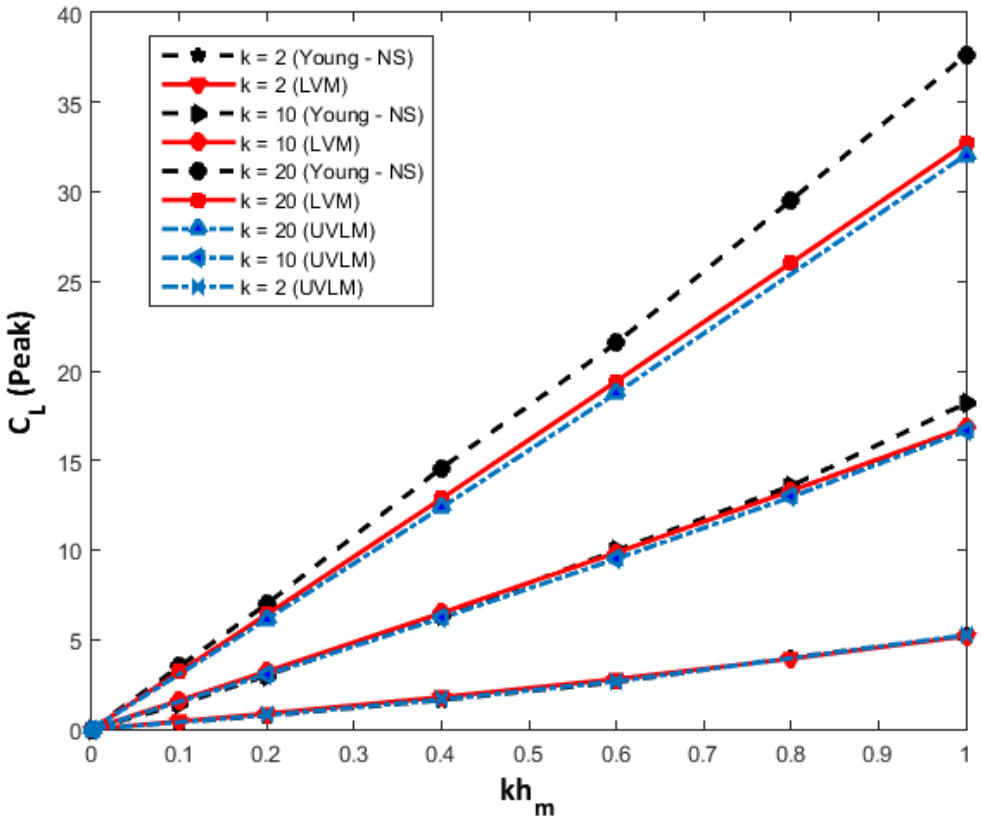

Fig. 3.2: Validation of UVLM with Navier-Stokes solver, comparison with LVM

The validation curve of UVLM merges with that of Navier-Stokes solver for low values of non-dimensional frequency *k*. With higher values of *k*, flow separation comes into play, which the UVLM solver is unable to take care of, and hence, shows large deviation from the results of Navier-Stokes solver, which takes flow separation into consideration, thereby accounting for a more accurate physics of the fluid flow. Also, the LVM solver is found to give closer result to Navier-Stokes solver than the UVLM solver. This might be because of the small time step of *dt*=0.0001 used in case of LVM as compared to *dt*=0.005 used for UVLM validation.

CHAPTER FOUR

COUPLING OF DUFFING EQUATION WITH UVLM SOLVER

4.1 Introduction

In the previous chapters, we have studied about the flow solvers and different structural models separately. But our goal is not to understand the behaviour of fluid flow separately, rather to understand how to model a structure so that it can interact appropriately with the fluid flow. So, our next job is to couple the structural model with the flow solver in order to study the fluid-structure interaction dynamics of the system.

FSI can be defined as the multi-physics coupling between the laws of fluid dynamics and structural mechanics. FSI can be stable or oscillatory. Oscillatory interactions can be sometimes catastrophic, especially in vibration prone structures like bridges. But in other cases we may also exploit the effects of FSI in designing a structure. So, FSI study is very important for the optimization of a structural system. Few applications of FSI includes the design of an aircraft, bridges, MAVs, peristaltic pumps, racing cars etc.

The basic principle of FSI is that the output from the fluid part (aerodynamic forces and moment) is the input to the structure part and the output from the structure part (displacement and velocity) is the input to the fluid part. We have seen previously that in order to solve for the fluid part, we have to take the aid of certain flow solvers. The flow solver that we will be using here is the UVLM solver. Again, we have also noticed that in order to solve for the structure part, we need to consider a physical model. The physical model that we will be considering here is the insect flight motor model proposed by Brennan *et al*. The mathematical expression for this physical model is basically a form of Duffing equation.

By observing the FSI dynamics, our target is to infer about the different types of dynamics that we are obtaining for different parameter values. In order to achieve the desired values of lift and drag, we can adjust the parameters and see the dynamics. Our main target is to do the fine tuning of these parameters so that we can model an insect wing properly in order to interact with the flow.

4.2 Duffing equation: Brennan's form

In the first chapter, we have already discussed about the insect flight motor model proposed by Brennan *et al*. We will be recapitulating the mathematical model here.

The governing mathematical equation that we will be using here is a second order differential equation of the non-dimensional displacement with respect to time. The equation is as follows:

$$\ddot{u} + \gamma\omega_0\dot{u} - \frac{\omega_0^2}{2}u(1-u^2) = \frac{P}{mL}\cos(\omega t) \qquad 4.1$$

Where, $u=\frac{y}{L}$, *y*=displacement, L= $\sqrt{\frac{2\left(1-\frac{b}{l}\right)}{\frac{b}{l^3}}}$ for $\frac{b}{l} < 1$ and the meanings of b and l have been given earlier in the first chapter . So *u* is the non-dimensional displacement parameter. Here, γ=damping factor, ω_0=natural frequency of the system, *P*=forcing amplitude, *m*=mass of the model, ω=forcing frequency, *t*=time. The term $\frac{P}{mL}$ can be replaced by *f* here, where *f* is the non-dimensional forcing amplitude.

When we take into account the aerodynamic forces coming from the fluid part, we have to replace the term $Pcos\omega t$ by the expression $(Pcos\omega t + Lift)$ in the right hand side of the above equation.

4.3 Parameter values

We have taken the values of few parameters from the paper regarding the insect flight motor model by Brennan *et al*. The values are as follows:

$$\frac{b}{l} = 0.9 \text{ and } \gamma = 0.168 \text{ (light damping case)}$$

The values of b and l are not mentioned in the paper. So, we have taken b=0.9 and thus l=1

We have also considered the values of other parameters as per our convenience since nothing is mentioned regarding this in the paper. So, we have taken ω_0=100 and ω=80

The mass is calculated from the geometry and by knowing the density of the solid material. The value of *Lift* is also calculated from the flow solver. Finally, we have varied the value of non-dimensional forcing amplitude (*f*) and studied the different dynamics due to the change of this parameter. A slightly different set of parameter values were used in order to do the time step convergence.

Though we are not absolutely sure about the parameter values that we have chosen, still these values can be taken as a starting point in order to study the FSI dynamics. After all, our job is fine tuning of the parameter values which we will be doing later on.

4.4 Time step convergence

We know that, convergence is basically arriving at a solution that is close to the exact solution. Now, the problem that we are dealing here is a time-dependent problem. So, time step convergence plays a crucial role in order to obtain the dynamics which is close to the actual one (here, the actual dynamics is not achievable due to the assumptions like inviscid flow etc. which is not the actual case in reality) and so before analysing the dynamics, we must go for the time step convergence.

When a solver converges, it means that it has found a solution to the system of equations at a specific time instant. If the time step is too big, or otherwise unsuitable, we may see that the next step also converges, but the solutions that we will be getting are incorrect. That means, different solutions will be obtained for different values of the time step interval (*dt*). So the time step size is modified by reducing its value until we obtain the same solution for two different time step sizes.

Any of the two time step sizes for which the solutions are matching can be used later on for the FSI study and analysis. If we choose to use the lower *dt* value, then we are expecting to have a higher resolution. On the other hand, we may opt for lower resolution by choosing the higher *dt* value in order to save our time. The lower resolution analysis can also help us to make a reliable prediction of the dynamics at a minimum computational cost.

We have already validated the UVLM code in the previous chapter. In the next page, the time step convergence graph is given. These graphs are basically the response of the coupled system.

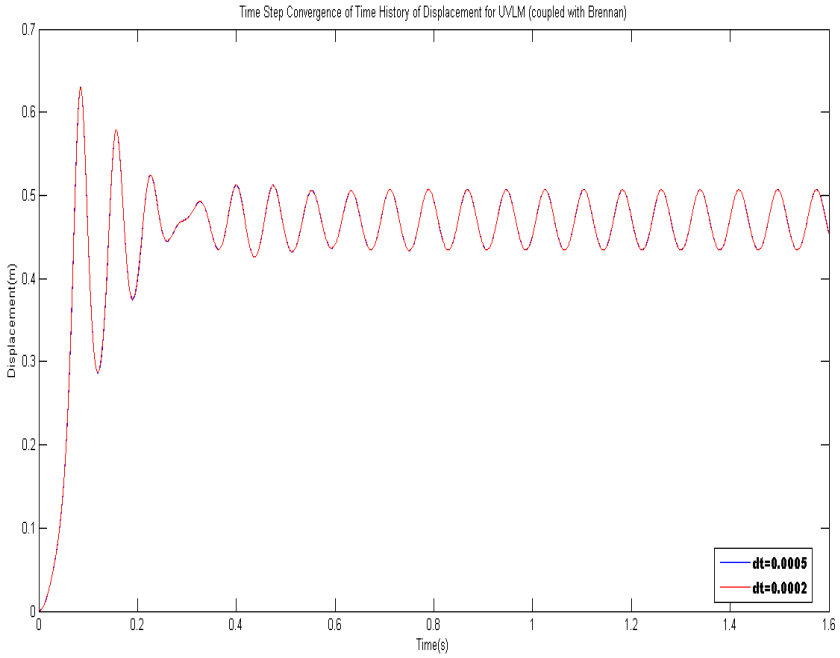

Fig. 4.1: Time step convergence

From the above figure, it is evident that the graphs of time history of displacement superimpose on one another for *dt*=0.0005 and *dt*=0.0002

In order to save our time, we have chosen *dt*=0.0005, i.e. lower resolution to study the FSI dynamics for different parameter values.

4.5 Results and discussions

After carrying out the time step convergence, our focus shifts onto our main topic of discussion, i.e. the study of the non-linear FSI dynamics. Our target here is to find out different dynamics by varying the non-dimensional forcing amplitude (*f*), more precisely, to observe the change from periodic behaviour to chaotic dynamics.

The range of *f* in which there is a marked change in the dynamics is evident from the figures given in the next few pages. We should narrow down the range in future and reach to a critical f value for which there is a transition from periodic to chaotic dynamics. But due to lack of time, the results that we have obtained are only given here.

Case 1: *f*=900

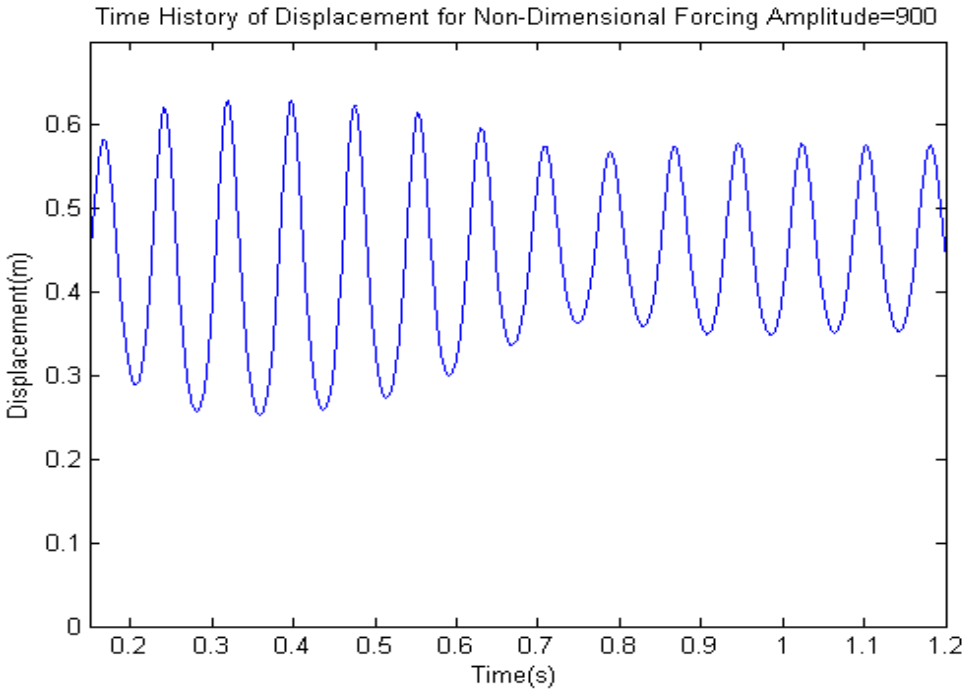

Fig. 4.2: Time history of displacement (*f*=900)

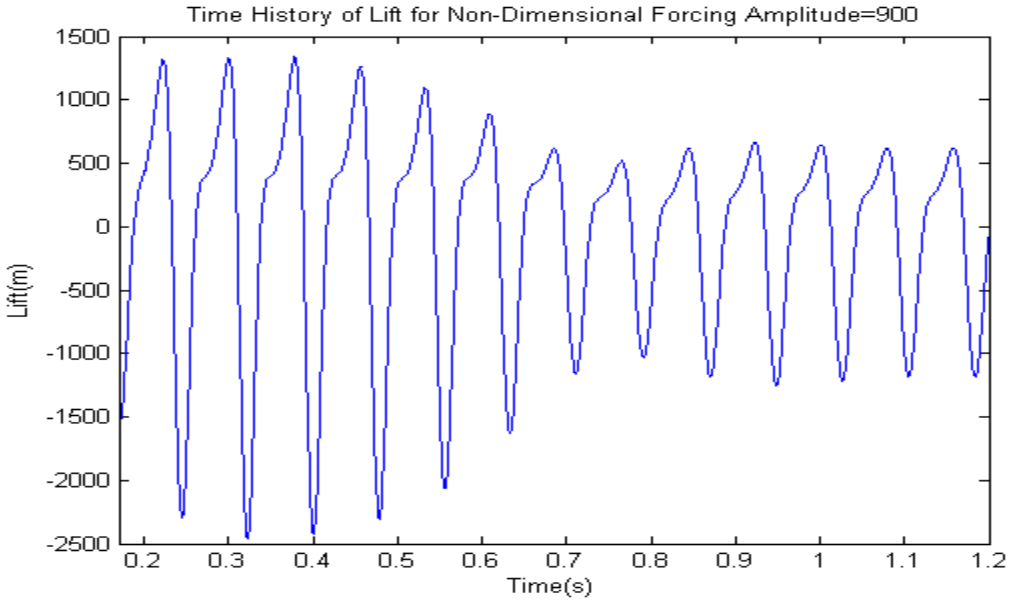

Fig. 4.3: Time history of lift (*f*=900)

From the above two figures, it is clear that the dynamics is of period 1 oscillation.

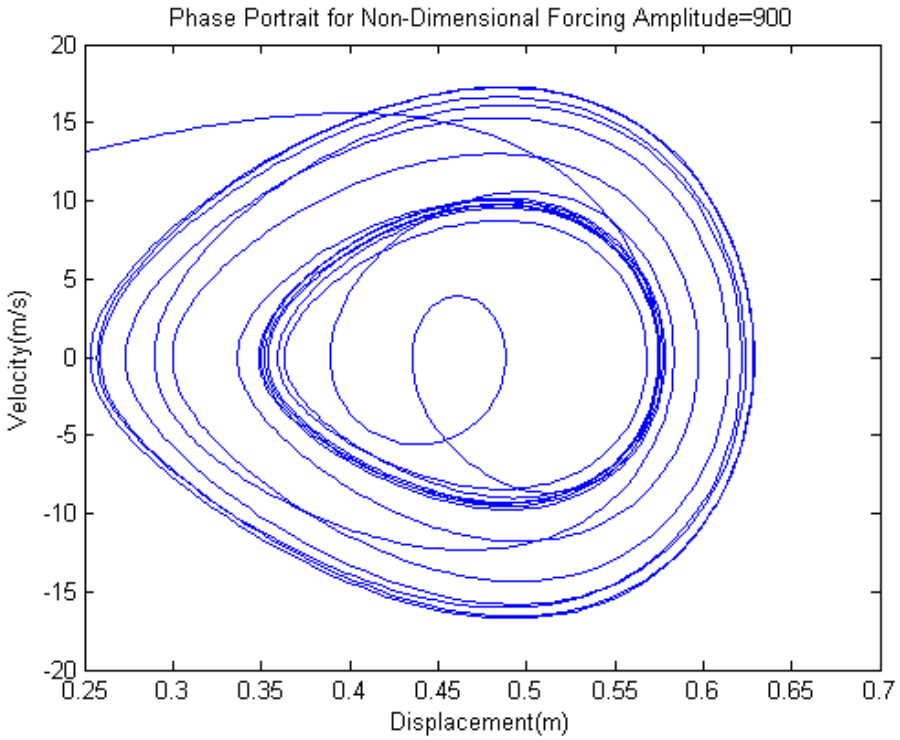

Fig. 4.4: Phase portrait (*f*=900)

The phase portrait also indicates a periodic oscillation in this case.

Case 2: *f*=915

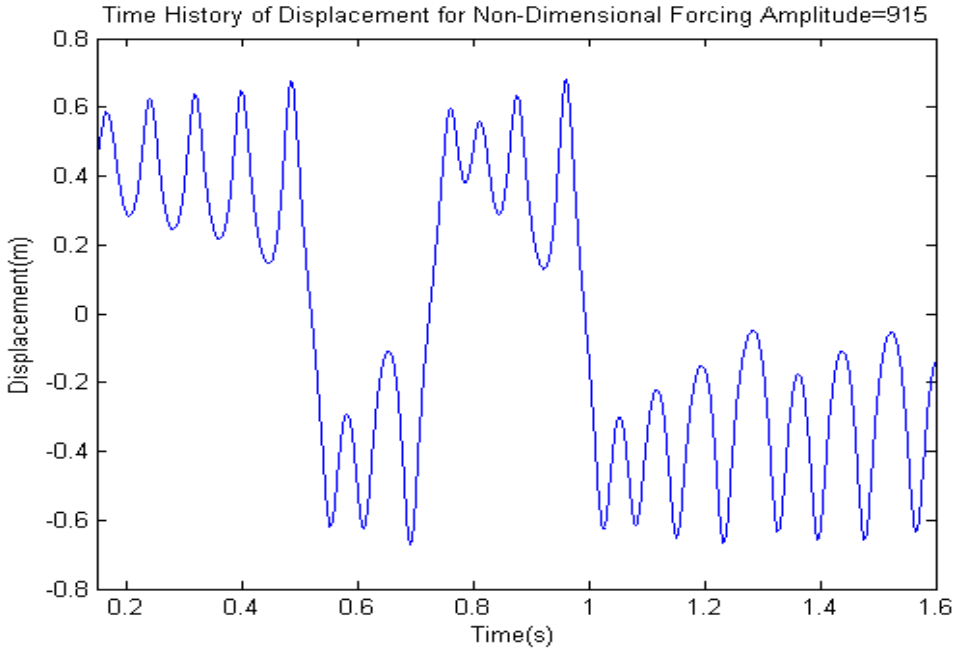

Fig. 4.5: Time history of displacement (*f*=915)

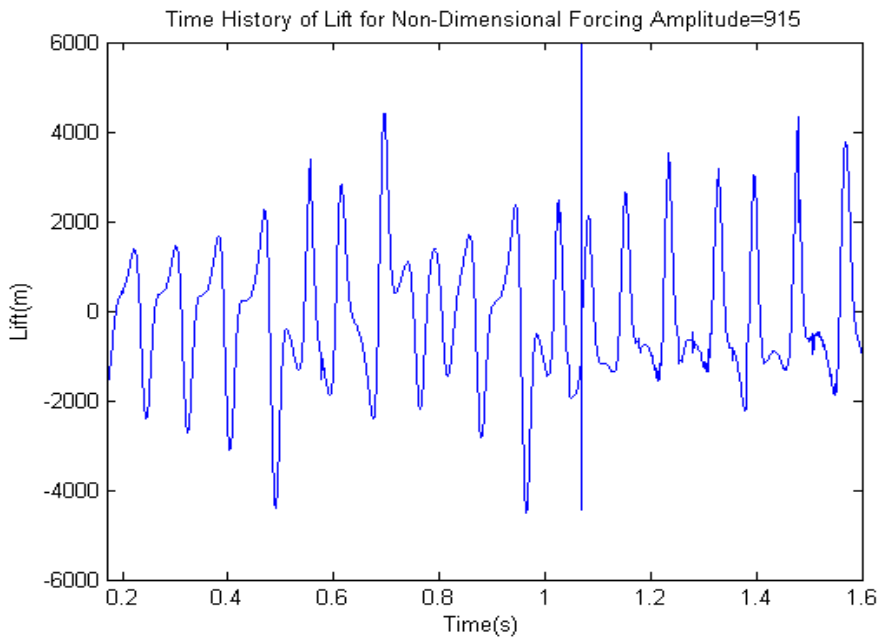

Fig. 4.6: Time history of lift (*f*=915)

From Fig. 4.5 and Fig. 4.6, we can say that, when we change the value of *f* from 900 to 915, the dynamics changes. The time history of displacement and lift both denote that the oscillation no longer remains a period 1 type. Rather from these figures, we may suspect that the dynamics denotes chaos. If we had plotted for longer time, then we could have surely told that this is chaos.

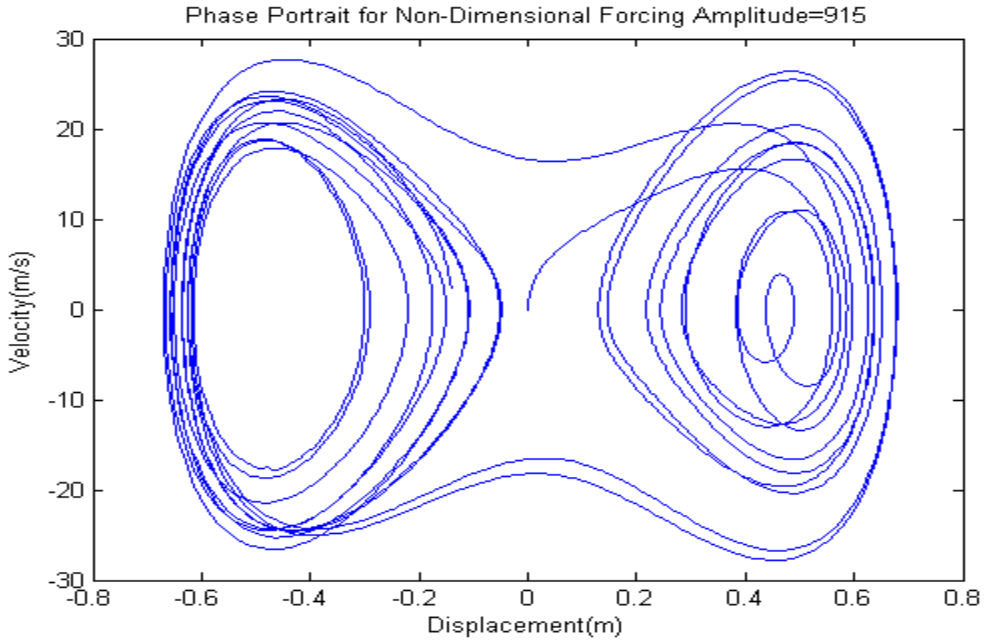

Fig. 4.7: Phase portrait (*f*=915)

The Phase Portrait given in Fig. 4.7 for f=915 denotes a double well dynamics. The particle moves within those two attractive wells. The dynamics can be said to be a heteroclinic orbit also. If we had not considered the effect of damping, then we should have got a homoclinic orbit instead.

For f=915, whether the dynamics indicates chaos or not is yet to be ascertained. But one thing is evident that there is a noticeable change in the dynamics. Further investigation is required regarding the dynamics and to find chaos which will be done in future.

CHAPTER FIVE

COUPLING OF NON-LINEAR AERO-ELASTIC MODEL HAVING PITCH AND PLUNGE DEGREES OF FREEDOM WITH UVLM SOLVER

5.1 Introduction

A non-linear aero-elastic model undergoing pitching and plunging motion can be successfully used to model self-sustained LCO, called flutter, of large flexible structures. Flutter is a dynamic instability of a structure resulting from the effect of the aerodynamic loads of a fluid flow. As the aerodynamic loads get coupled with the structural system, for some particular non-dimensional parameter values, it exhibits periodic motion with large amplitude and as such the phenomenon of flutter, at times, can have far reaching disastrous effects. In order to prevent or to have a precise knowledge and control over the onset of flutter, a thorough parametric study is required to determine the flutter limit. Also, it is worth mentioning that the same structural system behaves differently in presence of an additional external periodic forcing showing different routes to chaos.

In the present chapter, all these various aspects of the coupling of non-linear aero-elastic model having pitch and plunge DOF with the UVLM flow solver is explored.

5.2 Governing equations

The general equation of a structural model with non-linear springs in two DOF having pitch and plunge motion is given by:

$$m\ddot{h} + S_\alpha \ddot{\alpha} + C_h \dot{h} + K_h h + K_{h1} h^3 = -L(t) + F(t) \quad 5.1$$

$$S_\alpha \ddot{h} + I_\alpha \ddot{\alpha} + C_\alpha \dot{\alpha} + K_\alpha \alpha + K_{\alpha 1} \alpha^3 = M(t) \quad 5.2$$

Here, *F(t)* is the periodic external forcing which may be present on the structure at any time step. A schematic diagram of the airfoil section undergoing pitching and plunging motion in two dimension is shown:

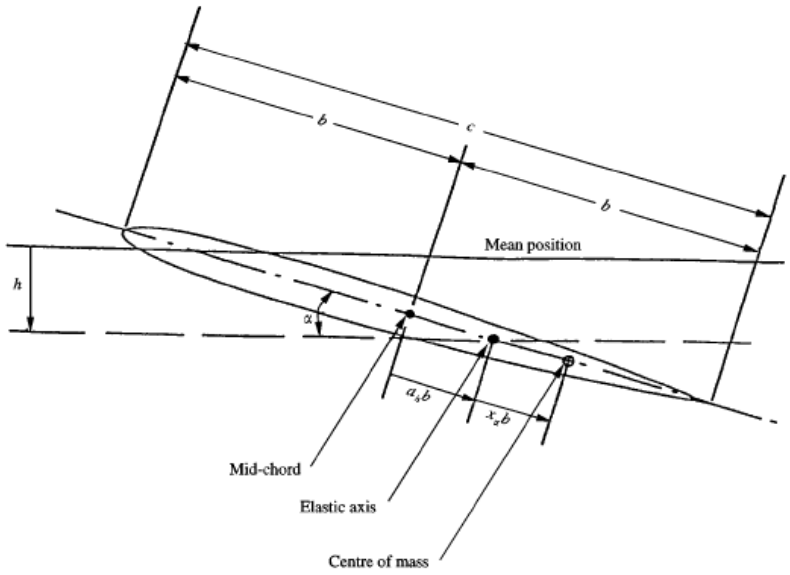

Fig. 5.1: Schematic of a 2 DOF airfoil motion (from Lee *et al*. (1999))

5.3 Onset of flutter

From the present work, the flutter limit, at which the airfoil starts LCO, has been found at U^*=5.0. This is in close agreement with the flutter limit suggested by different literatures. The dynamics of the system corresponding to U^*=5.0 are given below:

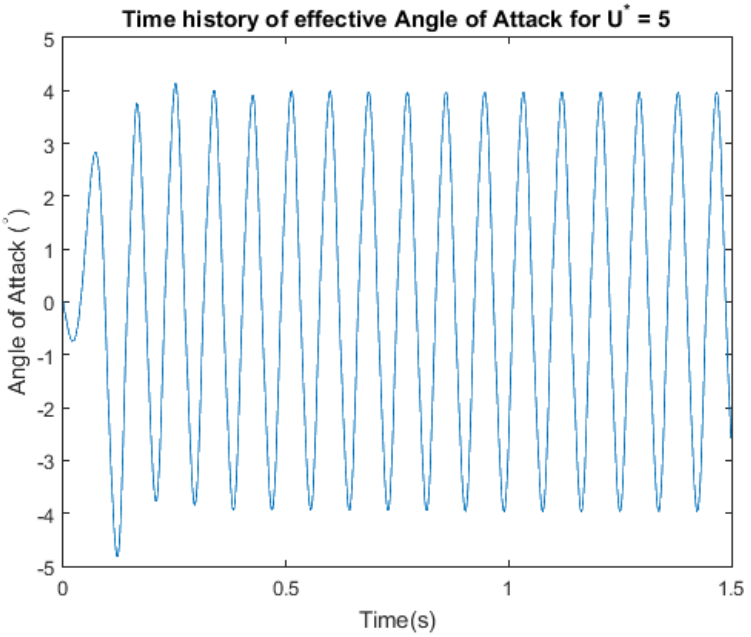

Fig. 5.2: Time history of angle of attack for U^*=5.0

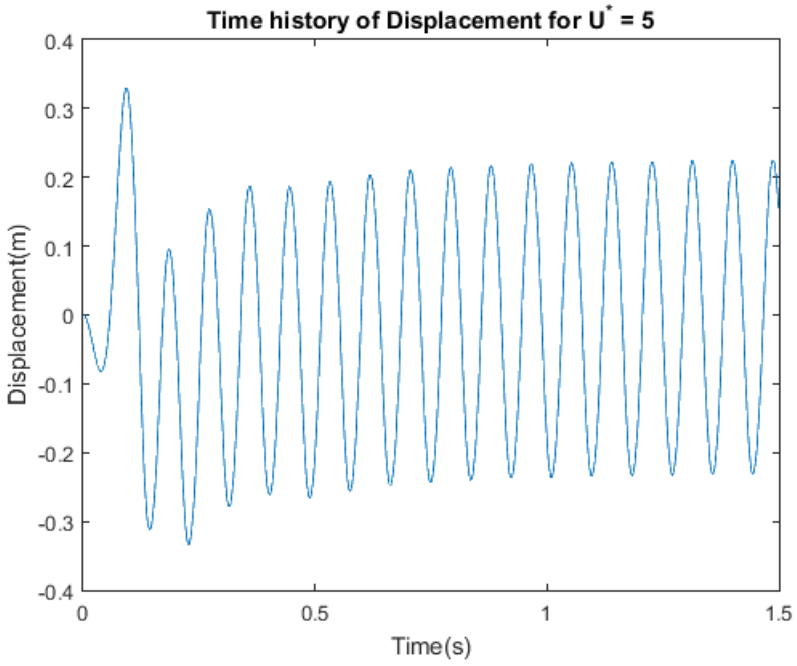

Fig. 5.3: Time history of displacement for *U**=5.0

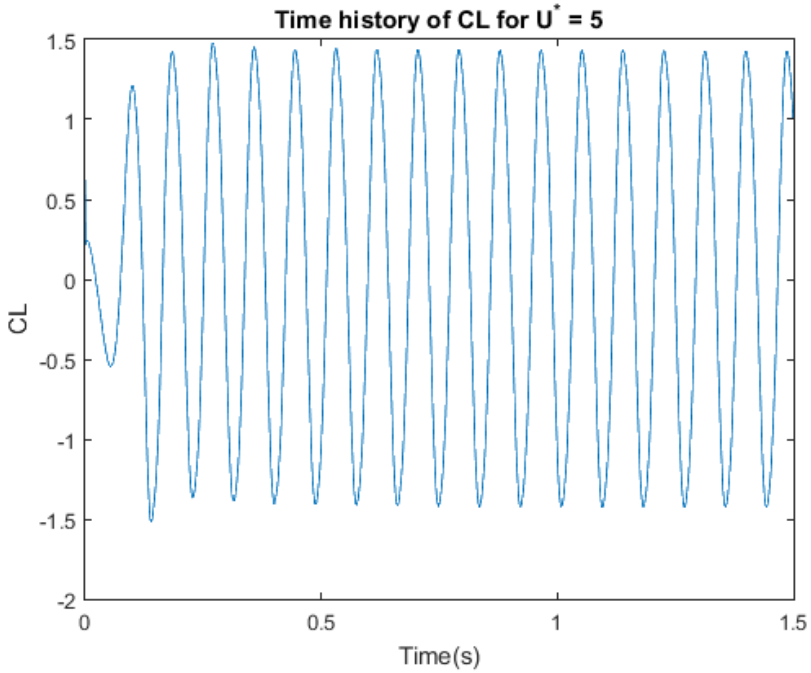

Fig. 5.4: Time history of CL for *U**=5.0

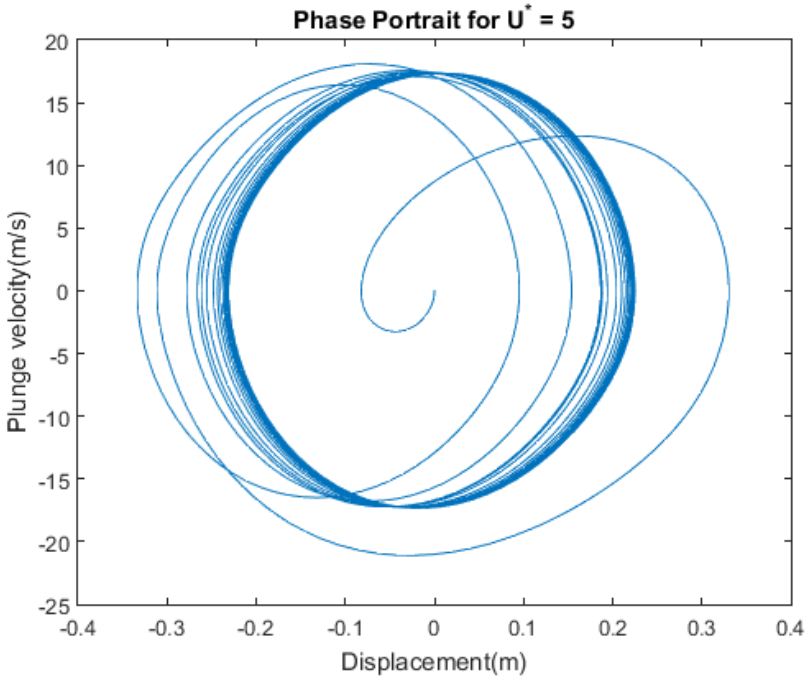

Fig. 5.5: Phase portrait for *U**=5.0

5.4 Behaviour under external periodic forcing

The dynamics of the non-linear aero-elastic model having pitch and plunge DOF coupled with the UVLM solver is studied under the influence of periodic external forcing. The time step convergence for the coupling of UVLM solver with non-linear aero-elastic model is not done owing to the large computational time required. The dynamics are studied with a time step of *dt*=0.001. The dynamics show a transition from periodic to quasi periodic behaviour as the dimensional forcing amplitude is increased and ultimately showing chaotic behavior for large forcing amplitude.

The dynamics resulting from different dimensional forcing amplitude are studied and conclusions are drawn from the Poincare sections and FFT of the displacement time history.

Case 1: Dimensional forcing amplitude = 50N

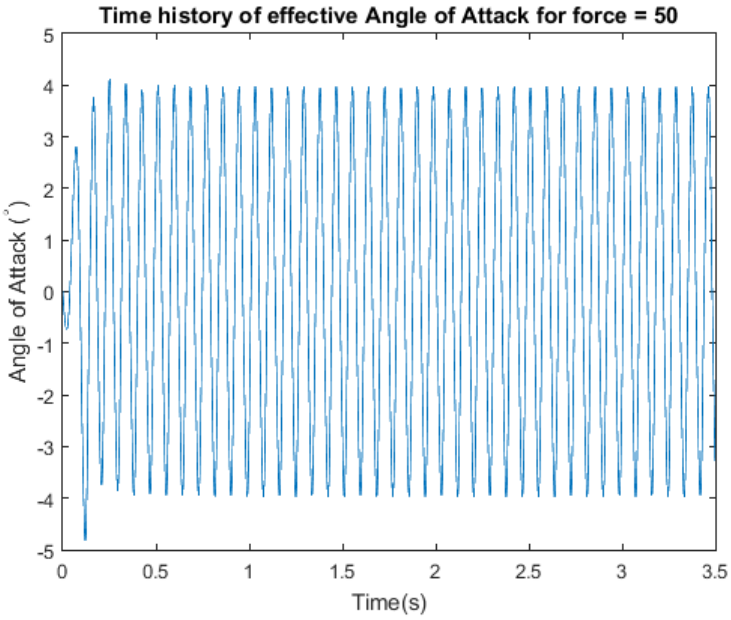

Fig. 5.6: Time history of angle of attack for dimensional force = 50N

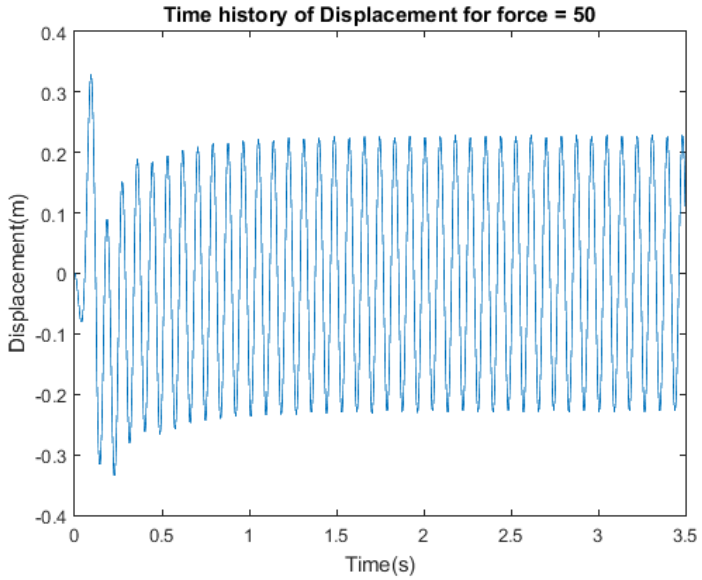

Fig. 5.7: Time history of displacement for dimensional force = 50N

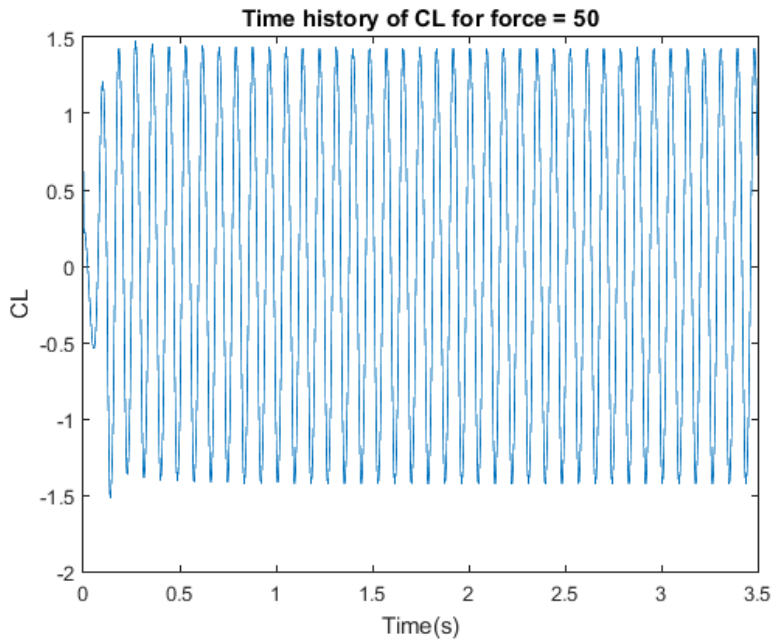

Fig. 5.8: Time history of CL for dimensional force = 50N

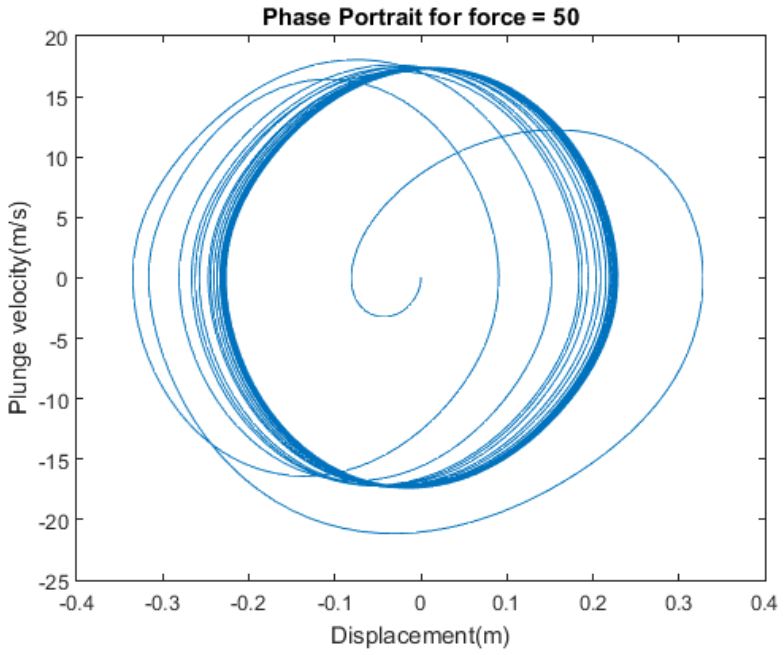

Fig. 5.9: Phase portrait for dimensional force = 50N

It is clearly seen that the dynamics under dimensional forcing amplitude of 50N show periodic oscillation.

Case 2: Dimensional forcing amplitude = 6000N

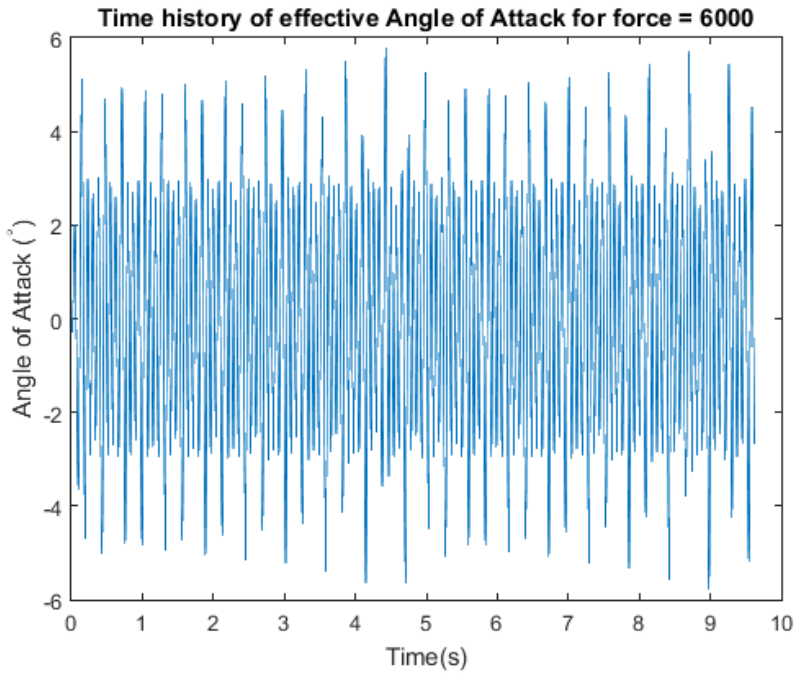

Fig. 5.10: Time history of angle of attack for dimensional force = 6000N

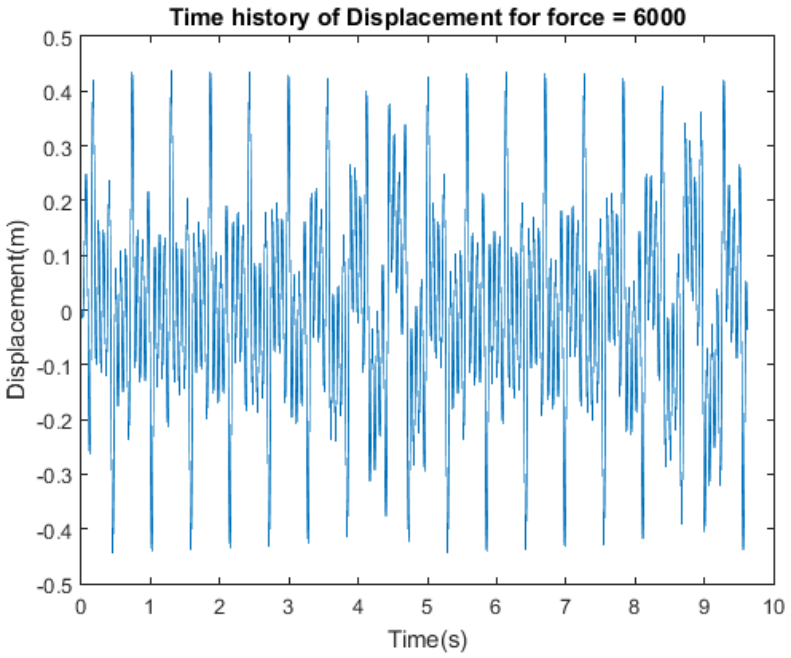

Fig. 5.11: Time history of displacement for dimensional force = 6000N

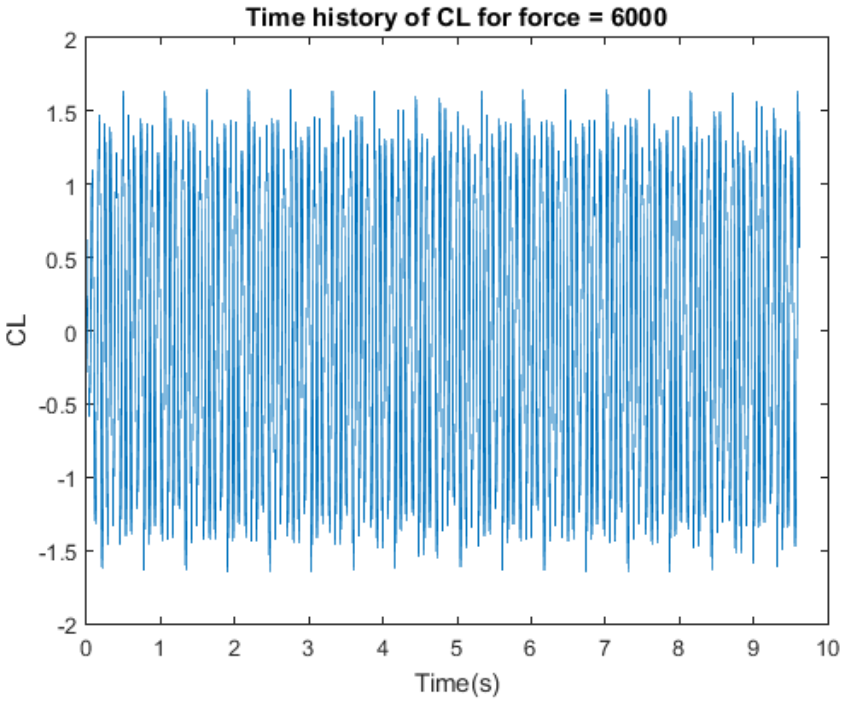

Fig. 5.12: Time history of CL for dimensional force = 6000N

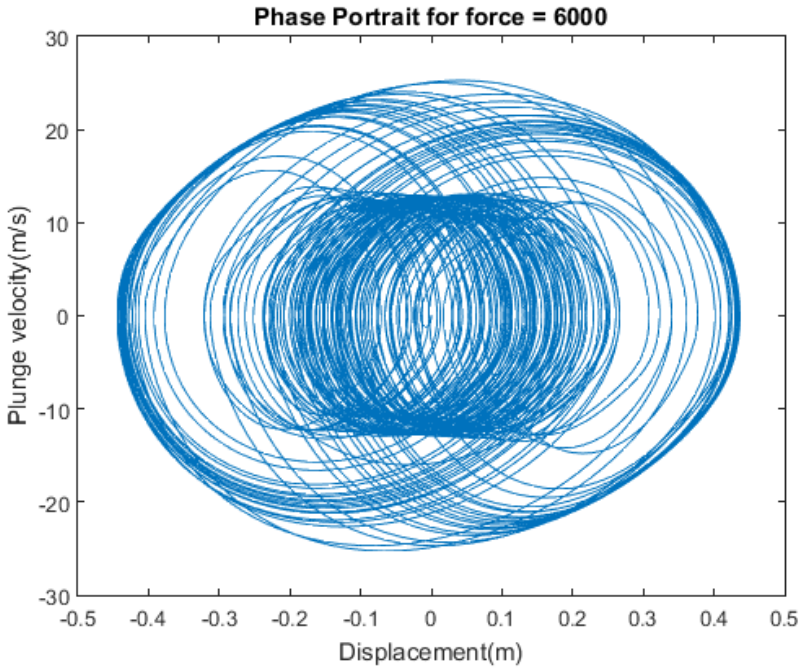

Fig. 5.13: Phase portrait for dimensional force = 6000N

As the dimensional forcing is kept on increasing, the dynamics of the system changes from periodic to quasi periodic oscillation. The phase space diagram shows

the projection of a torus on two dimension. To ascertain the quasi periodic dynamics of the system, Poincare section of phase portrait and FFT of plunge displacement is taken. The results are given below:

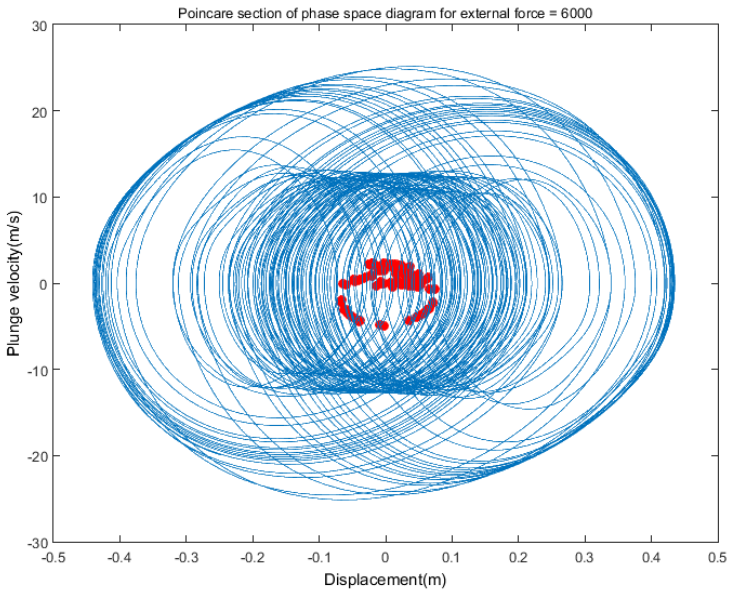

Fig. 5.14: Poincare section of phase portrait for dimensional force = 6000N

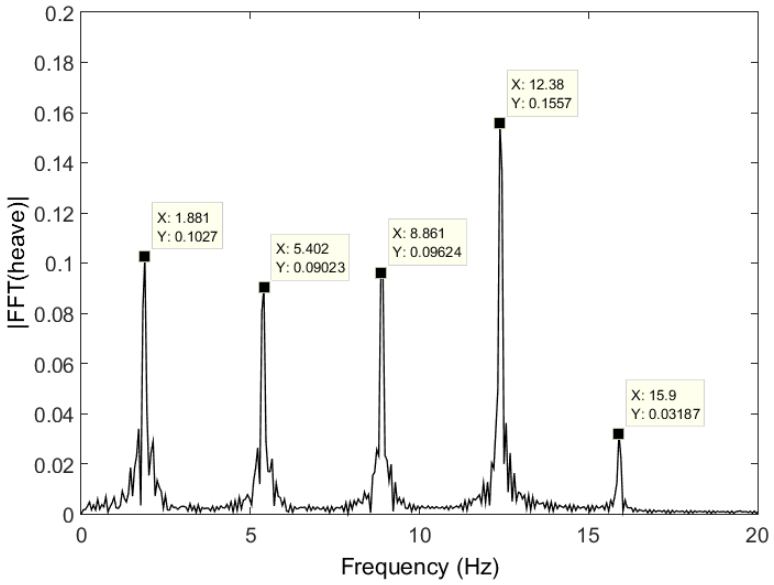

Fig. 5.15: FFT of plunge displacement for dimensional force = 6000N

The Poincare section shows a closed loop, which is expected in case of a torus projected phase space, while the FFT shows some peak frequencies, which are mutually incommensurate.

Case 3: Dimensional forcing amplitude = 7000N

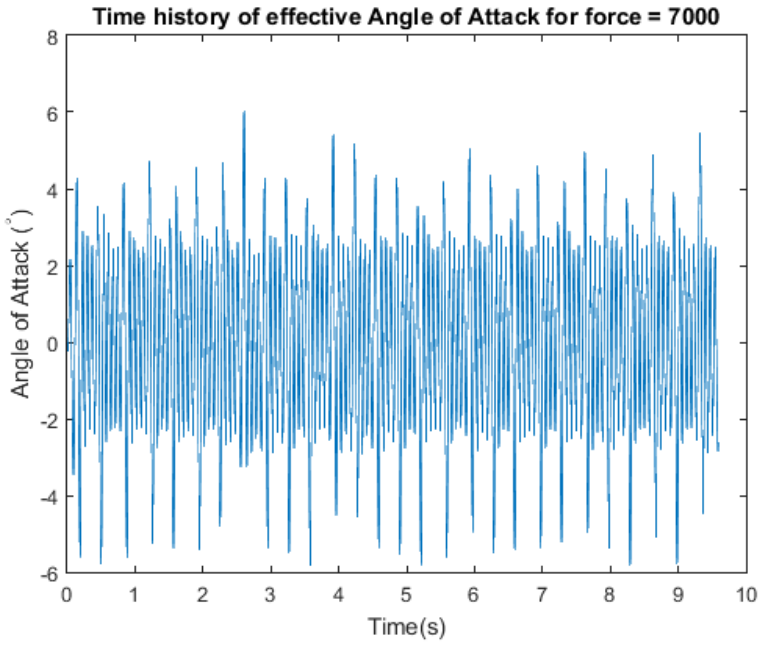

Fig. 5.16: Time history of angle of attack for dimensional force = 7000N

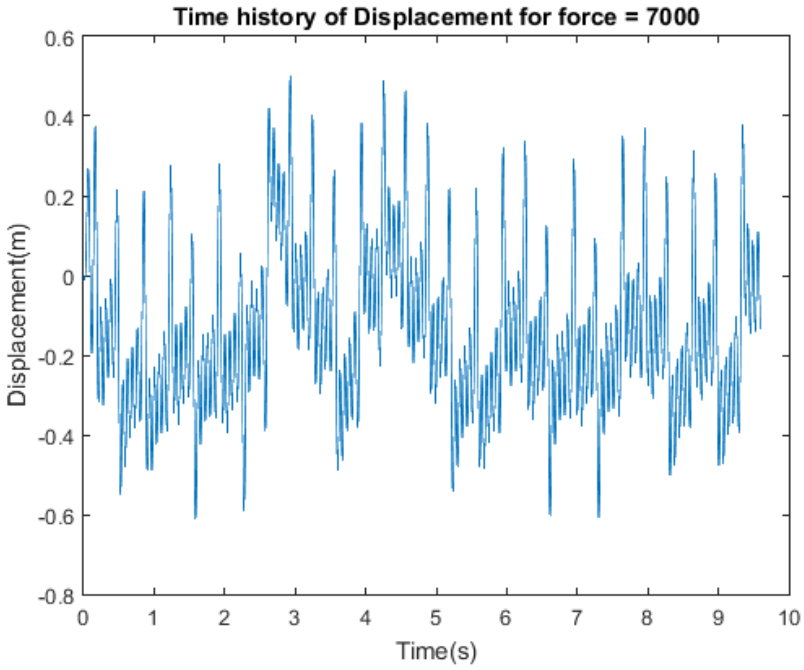

Fig. 5.17: Time history of displacement for dimensional force = 7000N

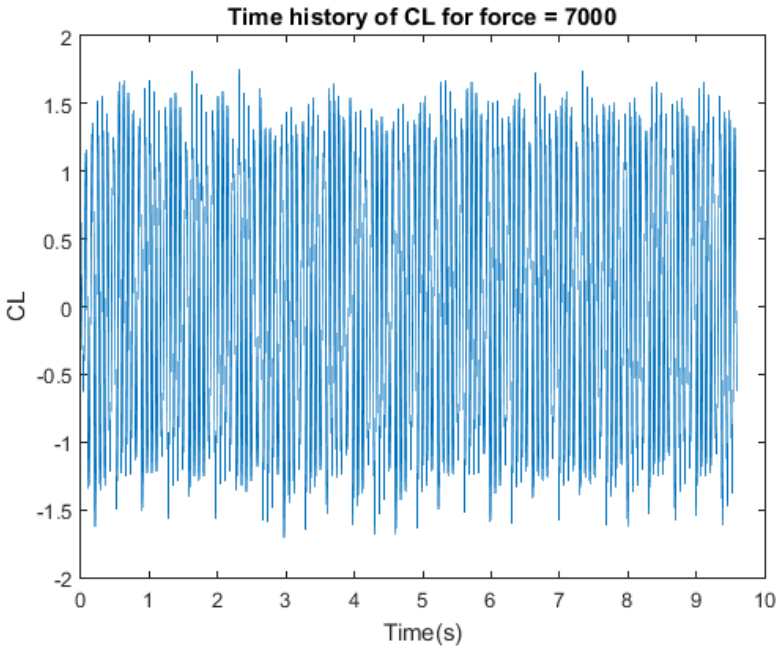

Fig. 5.18: Time history of CL for dimensional force = 7000N

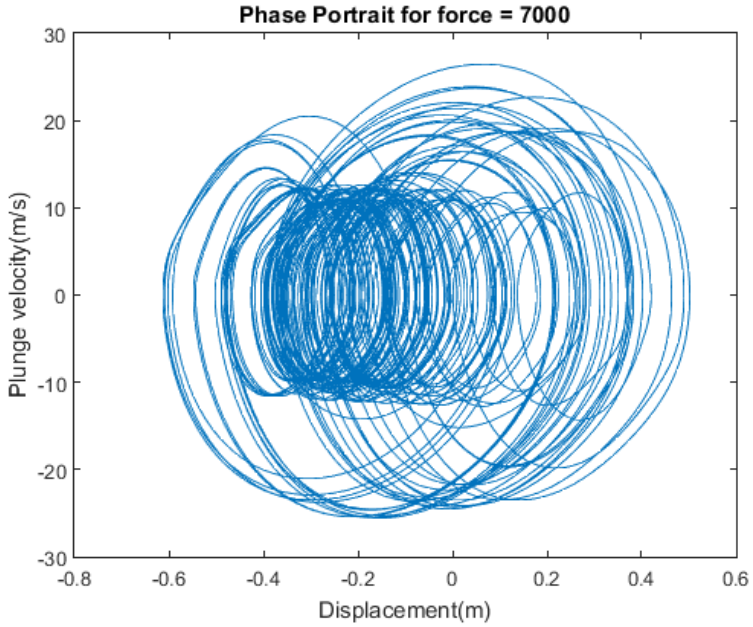

Fig. 5.19: Phase portrait for dimensional force = 7000N

For dimensional forcing amplitude 7000N, the dynamics show a transition from quasi periodic to chaotic nature.

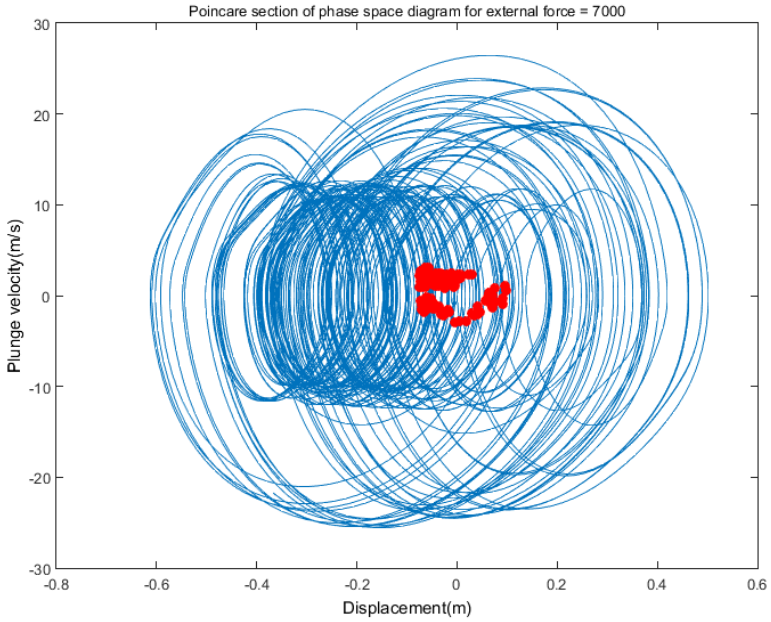

Fig. 5.20: Poincare section of phase space for dimensional force = 7000N

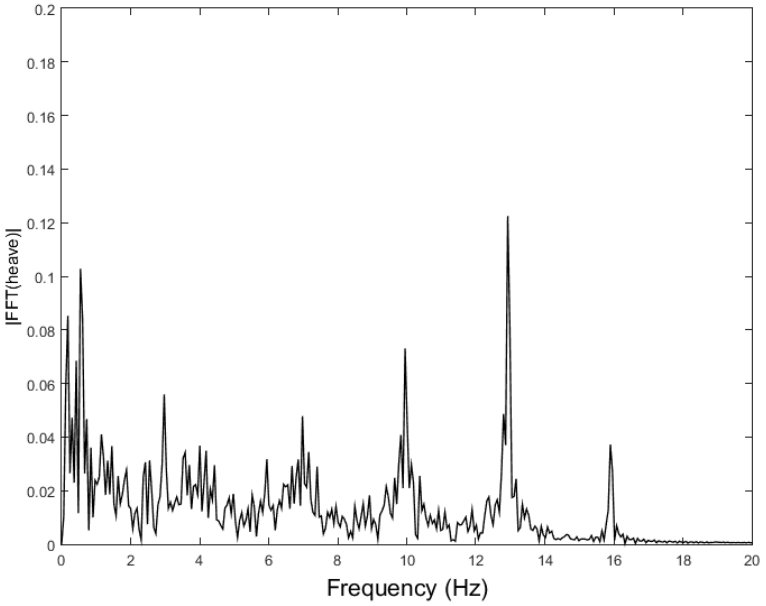

Fig. 5.21: FFT of plunge displacement for dimensional force = 7000N

The Poincare section does not form a closed loop. The points are somewhat scattered. Also the FFT shows a frequency spectrum which is

almost broadband in nature. Thus the dynamics show a transition from quasi periodic to chaotic.

Case 4: Dimensional forcing amplitude = 8000N

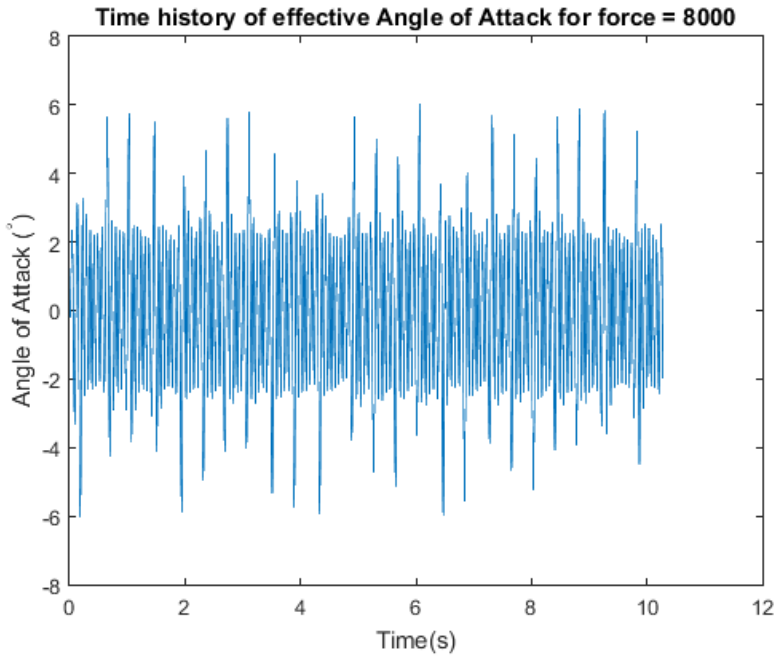

Fig. 5.22: Time history of angle of attack for dimensional force = 8000N

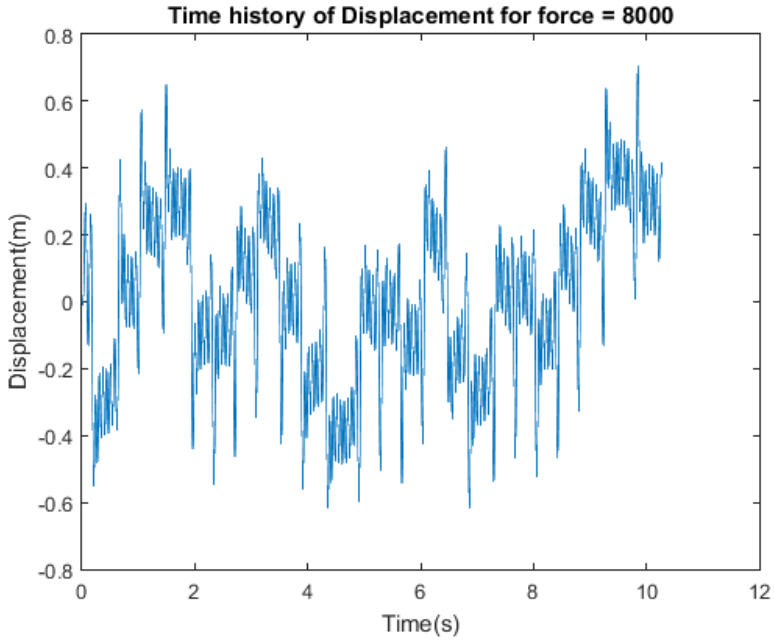

Fig. 5.23: Time history of displacement for dimensional force = 8000N

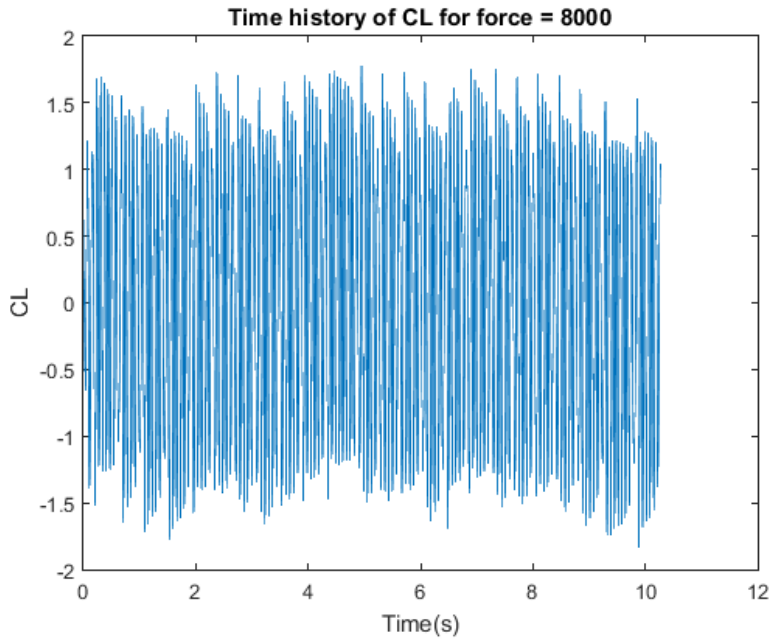

Fig. 5.24: Time history of CL for dimensional force = 8000N

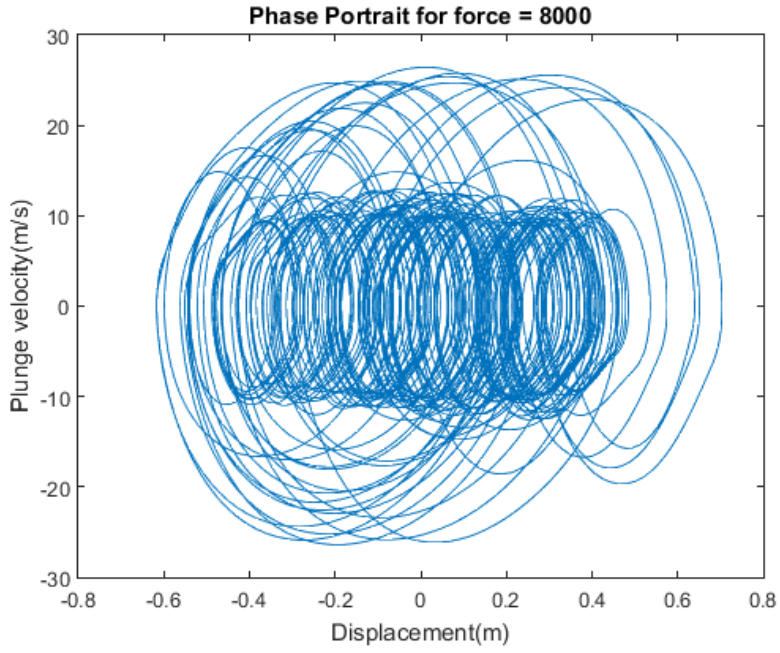

Fig. 5.25: Phase portrait for dimensional force = 8000N

The dynamics under external dimensional forcing amplitude of 8000N show almost chaotic behavior.

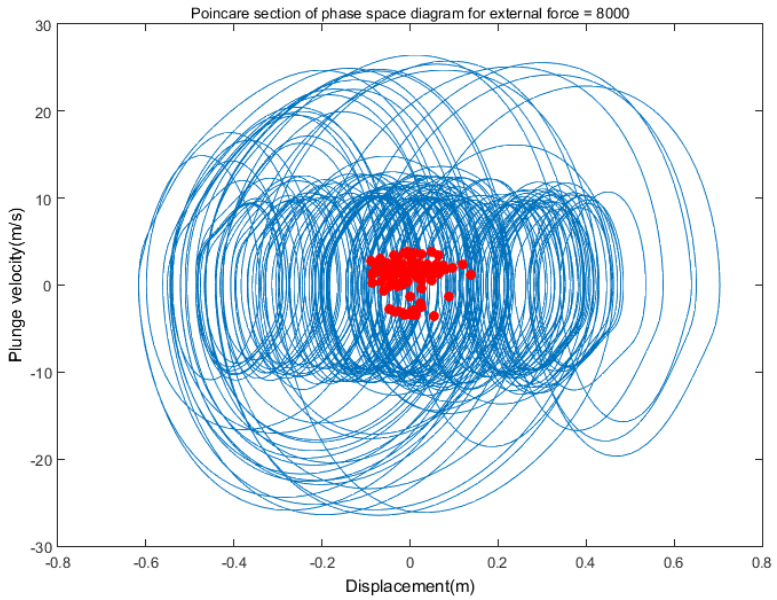

Fig. 5.26: Poincare section of phase space for dimensional force = 8000N

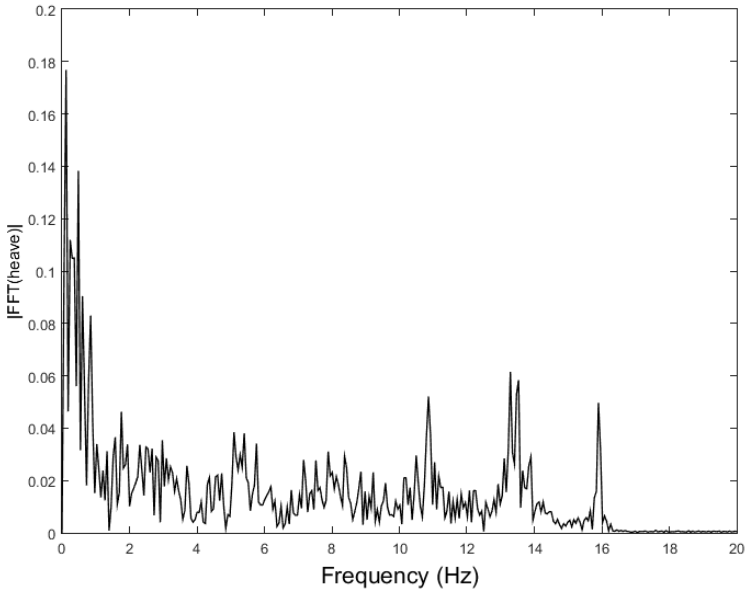

Fig. 5.27: FFT of plunge displacement for dimensional force = 8000N

The Poincare section gives scattered points on phase space and FFT shows broadband frequency spectrum. So the dynamics can be concluded to be chaotic.

CONCLUSION

The uncoupled Brennan's insect flight model shows a periodic oscillation of very small amplitude with non-zero mean for small non-dimensional forcing. With increase in non-dimensional forcing amplitude, transitional chaos is observed in the initial part thereafter exhibiting periodic oscillation with frequency of the external force. In the dipteran flight model with irrational non-linearity, some irregular kinks are observed at the peaks which keep on increasing with increase in non-dimensional forcing amplitude. Also, the phase space displays a double well structure. Under still higher non-dimensional forcing amplitude, the structural solver is found to fail.

The LVM code used in the present work has been validated against the Navier-Stokes solver and the simulation of flow by LVM for different values of *kh* has shown different wake vortex street patterns. Anti-Kármán pattern is observed for *kh* values of 0.1, 0.2 and 0.3 while deflected vortex street has been found for *kh* 0.6 and 1.0, which are in accordance to those obtained different literatures.

The newly developed MATLAB code during the project work, for UVLM flow solver, has been found to be valid for inviscid flows with small non-dimensional frequencies of the uncoupled structure. The future continuation of the work over the existing results are most likely to be carried on the same code unless it has to be discarded due to any discrepancies found in the results at any later stage.

The time step convergence of coupling of Brennan's insect flight model with UVLM solver has been achieved and different dynamical properties have been observed by varying the non-dimensional forcing amplitude. The dynamics show a trend from period one oscillation to intuitively suspected chaos. The justification for the observation of chaos is not possible in the present work due to the large computational time required for simulating over longer time span.

The main problem faced during the project is the long execution time required for the computational purposes with the coupled non-linear aero-elastic model having pitch and plunge DOF. As such, the time step convergence of coupling of UVLM with the non-linear aero-elastic model is not done, owing to the large time required for generating sufficient number of cycles with very small time step. Also, the possibility of reducing the number of time steps by increasing the natural frequency of the structure results in large flow velocities coming into play, making

the UVLM flow solver susceptible to failure. So, the second bifurcation point with the non-linear aero-elastic model is also not observed in the present work. Moreover, in presence of external periodic forcing, the non-linear aero-elastic model has mostly shown quasi-periodic dynamics. The sufficiently high dimensional forcing required for route to chaos is also not feasible to be fed into the flow solver and hence chaos was also not properly observed with the system.

REFERENCES

[1] John D. Anderson, Jr., *Fundamentals of Aerodynamics*, McGraw-Hill Inc.

[2] Joseph Katz, Allen Plotkin, *Low-Speed Aerodynamics*, McGraw-Hill Inc.

[3] Tuncer Cebeci, Max Platzer, Hsun Chen, Kuo-Cheng Chang, Jian P. Shao, *Analysis of Low-Speed Unsteady Airfoil Flows*, Horizons Publishing Inc.

[4] Marian Wiercigroch, Qingjie Cao, Yeping Xiong, *A novel model of dipteran flight mechanism*, Int. J. Dynam. Control (2013).

[5] M.J. Brennan, S.J. Elliott, P. Bonello, J.F.V. Vincent, *The ‘‘click’’ mechanism in dipteran flight: if it exists, then what effect does it have?*, Journal of Theoretical Biology (2003).

[6] Salil Harris, Sunetra Sarkar, *Flow-Field Dynamics of a Flexible Flapping Airfoil using a Navier-Stokes Solver*.

[7] S. Venkatesh, *Uncertainty quantification of an aeroelastic system under random gust using polynomial chaos expansion*, MS thesis at IIT Madras.

[8] B.H.K. Lee, L.Y. Jiang, *Flutter of an airfoil with a cubic restoring force*, Journal of Fluids and Structures (1999).